



A Gravitational-wave Measurement of the Hubble Constant Following the Second Observing Run of Advanced LIGO and Virgo

B. P. Abbott¹, R. Abbott¹, T. D. Abbott², S. Abraham³, F. Acernese^{4,5}, K. Ackley⁶, C. Adams⁷, R. X. Adhikari¹, V. B. Adya⁸, C. Affeldt^{9,10}, M. Agathos^{11,12}, K. Agatsuma¹³, N. Aggarwal¹⁴, O. D. Aguiar¹⁵, L. Aiello^{16,17}, A. Ain³, P. Ajith¹⁸, G. Allen¹⁹, A. Allocca^{20,21}, M. A. Aloy²², P. A. Altin⁸, A. Amato²³, S. Anand¹, A. Ananyeva¹, S. B. Anderson¹, W. G. Anderson²⁴, S. V. Angelova²⁵, S. Antier²⁶, S. Appert¹, K. Arai¹, M. C. Araya¹, J. S. Areeda²⁷, M. Arène²⁶, N. Arnaud^{28,29}, S. M. Aronson³⁰, K. G. Arun³¹, S. Ascenzi^{16,32}, G. Ashton⁶, S. M. Aston⁷, P. Astone³³, F. Aubin³⁴, P. Aufmuth¹⁰, K. AultO'Neal³⁵, C. Austin², V. Avendano³⁶, A. Avila-Alvarez²⁷, S. Babak²⁶, P. Bacon²⁶, F. Badaracco^{16,17}, M. K. M. Bader³⁷, S. Bae³⁸, J. Baird²⁶, P. T. Baker³⁹, F. Baldaccini^{40,41}, G. Ballardín²⁹, S. W. Ballmer⁴², A. Bals³⁵, S. Banagiri⁴³, J. C. Barayoga¹, C. Barbieri^{44,45}, S. E. Barclay⁴⁶, B. C. Barish¹, D. Barker⁴⁷, K. Barkett⁴⁸, S. Barnum¹⁴, F. Barone^{5,49}, B. Barr⁴⁶, L. Barsotti¹⁴, M. Barsuglia²⁶, D. Barta⁵⁰, J. Bartlett⁴⁷, I. Bartos³⁰, R. Bassiri⁵¹, A. Basti^{20,21}, M. Bawaj^{41,52}, J. C. Bayley⁴⁶, M. Bazzan^{53,54}, B. Bécsy⁵⁵, M. Bejger^{26,56}, I. Belahcene²⁸, A. S. Bell⁴⁶, D. Beniwal⁵⁷, M. G. Benjamin⁵⁸, B. K. Berger⁵¹, G. Bergmann^{9,10}, S. Bernuzzi¹¹, C. P. L. Berry⁵⁸, D. Bersanetti⁵⁹, A. Bertolini³⁷, J. Betzwieser⁷, R. Bhandare⁶⁰, J. Bidler²⁷, E. Biggs²⁴, I. A. Bilenko⁶¹, S. A. Bilgili³⁹, G. Billingsley¹, R. Birney²⁵, O. Birnholtz⁶², S. Biscans^{1,14}, M. Bischl^{63,64}, S. Biscoveanu¹⁴, A. Bisht¹⁰, M. Bitossi^{21,29}, M. A. Bizouard⁶⁵, J. K. Blackburn¹, J. Blackman⁴⁸, C. D. Blair⁷, D. G. Blair⁶⁶, R. M. Blair⁴⁷, S. Bloemen⁶⁷, F. Bobba^{68,69}, N. Bode^{9,10}, M. Boer⁶⁵, Y. Boetzel⁷⁰, G. Bogaert⁶⁵, F. Bondu⁷¹, R. Bonnand³⁴, P. Booker^{9,10}, B. A. Boom³⁷, R. Bork¹, V. Boschi²⁹, S. Bose³, V. Bossilkov⁶⁶, J. Bosveld⁶⁶, Y. Bouffanais^{53,54}, A. Bozzi²⁹, C. Bradaschia²¹, P. R. Brady²⁴, A. Bramley⁷, M. Branchesi^{16,17}, J. E. Brau⁷², M. Breschi¹¹, T. Briant⁷³, J. H. Briggs⁴⁶, F. Brighenti^{63,64}, A. Brillet⁶⁵, M. Brinkmann^{9,10}, P. Brockill²⁴, A. F. Brooks¹, J. Brooks²⁹, D. D. Brown⁵⁷, S. Brunett¹, A. Buikema¹⁴, T. Bulik⁷⁴, H. J. Bulten^{37,75}, A. Buonanno^{76,77}, D. Buskulic³⁴, C. Buy²⁶, R. L. Byer⁵¹, M. Cabero^{9,10}, L. Cadonati⁷⁸, G. Cagnoli⁷⁹, C. Cahillane¹, J. Calderón Bustillo⁶, T. A. Callister¹, E. Calloni^{5,80}, J. B. Camp⁸¹, W. A. Campbell⁶, M. Canepa^{59,82}, K. C. Cannon⁸³, H. Cao⁵⁷, J. Cao⁸⁴, G. Carapella^{68,69}, F. Carbognani²⁹, S. Caride⁸⁵, M. F. Carney⁵⁸, G. Carullo^{20,21}, J. Casanueva Diaz²¹, C. Casentini^{32,86}, S. Caudill³⁷, M. Cavaglia^{87,88}, F. Cavalieri²⁹, G. Cella²¹, P. Cerdá-Durán²², E. Cesarini^{32,89}, O. Chaibi⁶⁵, K. Chakravarti³, S. J. Chamberlin⁹⁰, M. Chan⁴⁶, S. Chao⁹¹, P. Charlton⁹², E. A. Chase⁵⁸, E. Chassande-Mottin²⁶, D. Chatterjee²⁴, M. Chaturvedi⁶⁰, B. D. Cheeseboro³⁹, H. Y. Chen⁹³, X. Chen⁶⁶, Y. Chen⁴⁸, H.-P. Cheng³⁰, C. K. Cheong⁹⁴, H. Y. Chia³⁰, F. Chiadini^{69,95}, A. Chincarini⁵⁹, A. Chiummo²⁹, G. Cho⁹⁶, H. S. Cho⁹⁷, M. Cho⁷⁷, N. Christensen^{65,98}, Q. Chu⁶⁶, S. Chua⁷³, K. W. Chung⁹⁴, S. Chung⁶⁶, G. Ciani^{53,54}, M. Cieślak⁵⁶, A. A. Ciobanu⁵⁷, R. Ciolfi^{54,99}, F. Cipriano⁶⁵, A. Cirone^{59,82}, F. Clara⁴⁷, J. A. Clark⁷⁸, P. Clearwater¹⁰⁰, F. Cleva⁶⁵, E. Coccia^{16,17}, P.-F. Cohadon⁷³, D. Cohen²⁸, M. Colleoni¹⁰¹, C. G. Collette¹⁰², C. Collins¹³, M. Colpi^{44,45}, L. R. Cominsky¹⁰³, M. Constancio, Jr.¹⁵, L. Conti⁵⁴, S. J. Cooper¹³, P. Corban⁷, T. R. Corbitt², I. Cordero-Carrión¹⁰⁴, S. Corezzi^{40,41}, K. R. Corley¹⁰⁵, N. Cornish⁵⁵, D. Corre²⁸, A. Corsi⁸⁵, S. Cortese²⁹, C. A. Costa¹⁵, R. Cotesta⁷⁶, M. W. Coughlin¹, S. B. Coughlin^{58,106}, J.-P. Coulon⁶⁵, S. T. Countryman¹⁰⁵, P. Couvares¹, P. B. Covas¹⁰¹, E. E. Cowan⁷⁸, D. M. Coward⁶⁶, M. J. Cowart⁷, D. C. Coyne¹, R. Coyne¹⁰⁷, J. D. E. Creighton²⁴, T. D. Creighton¹⁰⁸, J. Cripe², M. Croquette⁷³, S. G. Crowder¹⁰⁹, T. J. Cullen², A. Cumming⁴⁶, L. Cunningham⁴⁶, E. Cuoco²⁹, T. Dal Canton⁸¹, G. D'Álya¹¹⁰, B. D'Angelo^{59,82}, S. L. Danilishin^{9,10}, S. D'Antonio³², K. Danzmann^{9,10}, A. Dasgupta¹¹¹, C. F. Da Silva Costa³⁰, L. E. H. Datrier⁴⁶, V. Dattilo²⁹, I. Dave⁶⁰, M. Davies²⁸, D. Davis⁴², E. J. Daw¹¹², D. DeBra⁵¹, M. Deenadayalan³, J. Degallaix²³, M. De Laurentis^{5,80}, S. Deléglise⁷³, W. Del Pozzo^{20,21}, L. M. DeMarchi⁵⁸, N. Demos¹⁴, T. Dent¹¹³, R. De Pietri^{114,115}, R. De Rosa^{5,80}, C. De Rossi^{23,29}, R. DeSalvo¹¹⁶, O. de Varona^{9,10}, S. Dhurandhar³, M. C. Díaz¹⁰⁸, T. Dietrich³⁷, L. Di Fiore⁵, C. DiFronzo¹³, C. Di Giorgio^{68,69}, F. Di Giovanni²², M. Di Giovanni^{117,118}, T. Di Girolamo^{5,80}, A. Di Lieto^{20,21}, B. Ding¹⁰², S. Di Pace^{33,119}, I. Di Palma^{33,119}, F. Di Renzo^{20,21}, A. K. Divakarla³⁰, A. Dmitriev¹³, Z. Doctor⁹³, F. Donovan¹⁴, K. L. Dooley^{87,106}, S. Doravari³, I. Dorrington¹⁰⁶, T. P. Downes²⁴, M. Drago^{16,17}, J. C. Driggers⁴⁷, Z. Du⁸⁴, J.-G. Ducoin²⁸, P. Dupej⁴⁶, O. Durante^{68,69}, S. E. Dwyer⁴⁷, P. J. Easter⁶, G. Eddolls⁴⁶, T. B. Edo¹¹², A. Effler⁷, P. Ehrens¹, J. Eichholz⁸, S. S. Eikenberry³⁰, M. Eisenmann³⁴, R. A. Eisenstein¹⁴, L. Errico^{5,80}, R. C. Essick⁹³, H. Estelles¹⁰¹, D. Estevez³⁴, Z. B. Etienne³⁹, T. Etzel¹, M. Evans¹⁴, T. M. Evans⁷, V. Fafone^{16,32,86}, S. Fairhurst¹⁰⁶, X. Fan⁸⁴, S. Farinon⁵⁹, B. Farr⁷², W. M. Farr¹³, E. J. Fauchon-Jones¹⁰⁶, M. Favata³⁶, M. Fays¹¹², M. Fazio¹²⁰, C. Fee¹²¹, J. Feicht¹, M. M. Fejer⁵¹, F. Feng²⁶, A. Fernandez-Galiana¹⁴, I. Ferrante^{20,21}, E. C. Ferreira¹⁵, T. A. Ferreira¹⁵, F. Fidecaro^{20,21}, I. Fiori²⁹, D. Fiorucci^{16,17}, M. Fishbach⁹³, R. P. Fisher¹²², J. M. Fishner¹⁴, R. Fittipaldi^{69,123}, M. Fitz-Axen⁴³, V. Fiumara^{69,124}, R. Flaminio^{34,125}, M. Fletcher⁴⁶, E. Floden⁴³, E. Flynn²⁷, H. Fong⁸³, J. A. Font^{22,126}, P. W. F. Forsyth⁸, J.-D. Fournier⁶⁵, Francisco Hernandez Vivanco⁶, S. Frasca^{33,119}, F. Frasconi²¹, Z. Frei¹¹⁰, A. Freise¹³, R. Frey⁷², V. Frey²⁸, P. Fritschel¹⁴, V. V. Frolov⁷, G. Fronze¹²⁷, P. Fulda³⁰, M. Fyffe⁷, H. A. Gabbard⁴⁶, B. U. Gadre⁷⁶, S. M. Gaebel¹³, J. R. Gair¹²⁸, L. Gammaitoni⁴⁰, S. G. Gaonkar³, C. García-Quirós¹⁰¹, F. Garufi^{5,80}, B. Gateley⁴⁷, S. Gaudio³⁵, G. Gaur¹²⁹, V. Gayathri¹³⁰, G. Gemme⁵⁹, E. Genin²⁹, A. Gennai²¹, D. George¹⁹, J. George⁶⁰, L. Gergely¹³¹, S. Ghonge⁷⁸, Abhirup Ghosh⁷⁶, Archisman Ghosh³⁷, S. Ghosh²⁴, B. Giacomazzo^{117,118}, J. A. Giaime^{2,7}, K. D. Giardino⁷, D. R. Gibson¹³², K. Gill¹⁰⁵, L. Glover¹³³, J. Griesmer¹³⁴, P. Godwin⁹⁰, E. Goetz⁴⁷, R. Goetz³⁰, B. Goncharov⁶, G. González², J. M. Gonzalez Castro^{20,21}, A. Gopakumar¹³⁵, S. E. Gossan¹, M. Gosselin^{20,21,29}, R. Gouaty³⁴, B. Grace⁸, A. Grado^{5,136}, M. Granata²³, A. Grant⁴⁶, S. Gras¹⁴, P. Grassia¹, C. Gray⁴⁷, R. Gray⁴⁶

G. Greco^{63,64}, A. C. Green³⁰, R. Green¹⁰⁶, E. M. Gretarsson³⁵, A. Grimaldi^{117,118}, S. J. Grimm^{16,17}, P. Groot⁶⁷, H. Grote¹⁰⁶, S. Grunewald⁷⁶, P. Gruning²⁸, G. M. Guidi^{63,64}, H. K. Gulati¹¹¹, Y. Guo³⁷, A. Gupta⁹⁰, Anchal Gupta¹, P. Gupta³⁷, E. K. Gustafson¹, R. Gustafson¹⁵⁷, L. Haegel¹⁰¹, O. Halim^{16,17}, B. R. Hall¹³⁸, E. D. Hall¹⁴, E. Z. Hamilton¹⁰⁶, G. Hammond⁴⁶, M. Haney⁷⁰, M. M. Hanke^{9,10}, J. Hanks⁴⁷, C. Hanna⁹⁰, M. D. Hannam¹⁰⁶, O. A. Hannuksela⁹⁴, T. J. Hansen³⁵, J. Hanson⁷, T. Harder⁶⁵, T. Hardwick², K. Haris¹⁸, J. Harms^{16,17}, G. M. Harry¹³⁹, I. W. Harry¹⁴⁰, R. K. Hasskew⁷, C. J. Haster¹⁴, K. Haughian⁴⁶, F. J. Hayes⁴⁶, J. Healy⁶², A. Heidmann⁷³, M. C. Heintze⁷, H. Heitmann⁶⁵, F. Hellman¹⁴¹, P. Hello²⁸, G. Hemming²⁹, M. Hendry⁴⁶, I. S. Heng⁴⁶, J. Hennig^{9,10}, M. Heurs^{9,10}, S. Hild⁴⁶, T. Hinderer^{37,142,143}, S. Hochheim^{9,10}, D. Hofman²³, A. M. Hologado¹⁹, N. A. Holland⁸, K. Holt⁷, D. E. Holz⁹³, P. Hopkins¹⁰⁶, C. Horst²⁴, J. Hough⁴⁶, E. J. Howell⁶⁶, C. G. Hoy¹⁰⁶, Y. Huang¹⁴, M. T. Hübner⁶, E. A. Huerta¹⁹, D. Huet²⁸, B. Hughey³⁵, V. Hui³⁴, S. Husa¹⁰¹, S. H. Huttner⁴⁶, T. Huynh-Dinh⁷, B. Idzkowski⁷⁴, A. Iess^{32,86}, H. Inchauspe³⁰, C. Ingram⁵⁷, R. Inta⁸⁵, G. Intini^{33,119}, B. Irwin¹²¹, H. N. Isa⁴⁶, J.-M. Isac⁷³, M. Isi¹⁴, B. R. Iyer¹⁸, T. Jacqmin⁷³, S. J. Jadhav¹⁴⁴, K. Jani⁷⁸, N. N. Janthalur¹⁴⁴, P. Jaranowski¹⁴⁵, D. Jariwala³⁰, A. C. Jenkins¹⁴⁶, J. Jiang³⁰, D. S. Johnson¹⁹, A. W. Jones¹³, D. I. Jones¹⁴⁷, J. D. Jones⁴⁷, R. Jones⁴⁶, R. J. G. Jonker³⁷, L. Ju⁶⁶, J. Junker^{9,10}, C. V. Kalaghatgi¹⁰⁶, V. Kalogera⁵⁸, B. Kamai¹, S. Kandhasamy³, G. Kang³⁸, J. B. Kanner¹, S. J. Kapadia²⁴, C. Karathanasis¹⁴⁸, S. Karki⁷², R. Kashyap¹⁸, M. Kasprzak¹, S. Katsanevas²⁹, E. Katsavounidis¹⁴, W. Katzman⁷, S. Kaufer¹⁰, K. Kawabe⁴⁷, N. V. Keerthana³, F. Kéfélian⁶⁵, D. Keitel¹⁴⁰, R. Kennedy¹¹², J. S. Key¹⁴⁹, F. Y. Khalili⁶¹, I. Khan^{16,32}, S. Khan^{9,10}, E. A. Khazanov¹⁵⁰, N. Khetan^{16,17}, M. Khursheed⁶⁰, N. Kijbunchoo⁸, Chunglee Kim¹⁵¹, J. C. Kim¹⁵², K. Kim⁹⁴, W. Kim⁵⁷, W. S. Kim¹⁵³, Y.-M. Kim¹⁵⁴, C. Kimball⁵⁸, P. J. King⁴⁷, M. Kinley-Hanlon⁴⁶, R. Kirchhoff^{9,10}, J. S. Kissel⁴⁷, L. Kleybolte¹³⁴, J. H. Klika²⁴, S. Klimenko³⁰, T. D. Knowles³⁹, P. Koch^{9,10}, S. M. Koehlenbeck^{9,10}, G. Koekoek^{37,155}, S. Koley³⁷, V. Kondrashov¹, A. Kontos¹⁵⁶, N. Koper^{9,10}, M. Korobko¹³⁴, W. Z. Korth¹, M. Kovalam⁶⁶, D. B. Kozak¹, C. Krämer^{9,10}, V. Kringel^{9,10}, N. Krishnendu³¹, A. Królak^{157,158}, N. Krupinski²⁴, G. Kuehn^{9,10}, A. Kumar¹⁴⁴, P. Kumar¹⁵⁹, Rahul Kumar⁴⁷, Rakesh Kumar¹¹¹, L. Kuo⁹¹, A. Kutynia¹⁵⁷, S. Kwang²⁴, B. D. Lackey⁷⁶, D. Laghi^{20,21}, K. H. Lai⁹⁴, T. L. Lam⁹⁴, M. Landry⁴⁷, B. B. Lane¹⁴, R. N. Lang¹⁶⁰, J. Lange⁶², B. Lantz⁵¹, R. K. Lanza¹⁴, A. Lartaux-Vollard²⁸, P. D. Lasky⁶, M. Laxen⁷, A. Lazzarini¹, C. Lazzaro⁵⁴, P. Leaci^{33,119}, S. Leavey^{9,10}, Y. K. Lecoeuche⁴⁷, C. H. Lee⁹⁷, H. K. Lee¹⁶¹, H. M. Lee¹⁶², H. W. Lee¹⁵², J. Lee⁹⁶, K. Lee⁴⁶, J. Lehmann^{9,10}, A. K. Lenon³⁹, N. Leroy²⁸, N. Letendre³⁴, Y. Levin⁶, A. Li⁹⁴, J. Li⁸⁴, K. J. L. Li⁹⁴, T. G. F. Li⁹⁴, X. Li⁴⁸, F. Lin⁶, F. Linde^{37,163}, S. D. Linker¹³³, T. B. Littenberg¹⁶⁴, J. Liu⁶⁶, X. Liu²⁴, M. Llorens-Monteagudo²², R. K. L. Lo¹⁹⁴, L. T. London¹⁴, A. Longo^{165,166}, M. Lorenzini^{16,17}, V. Lorette¹⁶⁷, M. Lormand⁷, G. Losurdo²¹, J. D. Lough^{9,10}, C. O. Lousto⁶², G. Lovelace²⁷, M. E. Lower¹⁶⁸, H. Lück^{9,10}, D. Lumaca^{32,86}, A. P. Lundgren¹⁴⁰, R. Lynch¹⁴, Y. Ma⁴⁸, R. Macas¹⁰⁶, S. Macfoy²⁵, M. MacInnis¹⁴, D. M. Macleod¹⁰⁶, A. Macquet⁶⁵, I. Magaña Hernandez²⁴, F. Magaña-Sandoval³⁰, R. M. Magee⁹⁰, E. Majorana³³, I. Maksimovic¹⁶⁷, A. Malik⁶⁰, N. Man⁶⁵, V. Mandic⁴³, V. Mangano^{33,46,119}, G. L. Mansell^{14,47}, M. Manske²⁴, M. Mantovani²⁹, M. Mapelli^{53,54}, F. Marchesoni^{41,52}, F. Marion³⁴, S. Márka¹⁰⁵, Z. Márka¹⁰⁵, C. Markakis¹⁹, A. S. Markosyan⁵¹, A. Markowitz¹, E. Maros¹, A. Marquina¹⁰⁴, S. Marsat²⁶, F. Martelli^{63,64}, I. W. Martin⁴⁶, R. M. Martin³⁶, V. Martinez⁷⁹, D. V. Martynov¹³, H. Masalehdan¹³⁴, K. Mason¹⁴, E. Massera¹¹², A. Masserot³⁴, T. J. Massinger¹, M. Masso-Reid⁴⁶, S. Mastrogiovanni²⁶, A. Matas⁷⁶, F. Matichard^{1,14}, L. Matone¹⁰⁵, N. Mavalvala¹⁴, J. J. McCann⁶⁶, R. McCarthy⁴⁷, D. E. McClelland⁸, S. McCormick⁷, L. McCuller¹⁴, S. C. McGuire¹⁶⁹, C. McIsaac¹⁴⁰, J. McIver¹, D. J. McManus⁸, T. McRae⁸, S. T. McWilliams³⁹, D. Meacher²⁴, G. D. Meadors⁶, M. Mehmet^{9,10}, A. K. Mehta¹⁸, J. Meidam³⁷, E. Mejuto Villa^{69,116}, A. Melatos¹⁰⁰, G. Mendell⁴⁷, R. A. Mercer²⁴, L. Mereni²³, K. Merfeld⁷², E. L. Merilh⁴⁷, M. Merzougui⁶⁵, S. Meshkov¹, C. Messenger⁴⁶, C. Messick⁹⁰, F. Messina^{44,45}, R. Metzdorff⁷³, P. M. Meyers¹⁰⁰, F. Meylahn^{9,10}, A. Miani^{117,118}, H. Miao¹³, C. Michel²³, H. Middleton¹⁰⁰, L. Milano^{5,80}, A. L. Miller^{30,33,119}, M. Millhouse¹⁰⁰, J. C. Mills¹⁰⁶, M. C. Milovich-Goff¹³³, O. Minazzoli^{65,170}, Y. Minenkov³², A. Mishkin³⁰, C. Mishra¹⁷¹, T. Mistry¹¹², S. Mitra³, V. P. Mitrofanov⁶¹, G. Mitselmakher³⁰, R. Mittleman¹⁴, G. Mo⁹⁸, D. Moffa¹²¹, K. Mogushi⁸⁷, S. R. P. Mohapatra¹⁴, M. Molina-Ruiz¹⁴¹, M. Mondin¹³³, M. Montani^{63,64}, C. J. Moore¹³, D. Moraru⁴⁷, F. Morawski⁵⁶, G. Moreno⁴⁷, S. Morisaki⁸³, B. Mours³⁴, C. M. Mow-Lowry¹³, F. Muciaccia^{33,119}, Arunava Mukherjee^{9,10}, D. Mukherjee²⁴, S. Mukherjee¹⁰⁸, Subroto Mukherjee¹¹¹, N. Mukund^{3,9,10}, A. Mullavey⁷, J. Munch⁵⁷, E. A. Muñoz⁴², M. Muratore³⁵, P. G. Murray⁴⁶, A. Nagar^{89,127,172}, I. Nardecchia^{32,86}, L. Naticchioni^{33,119}, R. K. Nayak¹⁷³, B. F. Neil⁶⁶, J. Neilson^{69,116}, G. Nelemans^{37,67}, T. J. N. Nelson⁷, M. Nery^{9,10}, A. Neunzert¹³⁷, L. Nevin¹, K. Y. Ng¹⁴, S. Ng⁵⁷, C. Nguyen²⁶, P. Nguyen⁷², D. Nichols^{37,142}, S. A. Nichols², S. Nissanke^{37,142}, F. Nocera²⁹, C. North¹⁰⁶, L. K. Nuttall¹⁴⁰, M. Obergaulinger^{22,174}, J. Oberling⁴⁷, B. D. O'Brien³⁰, G. Oganessian^{16,17}, G. H. Ogin¹⁷⁵, J. J. Oh¹⁵³, S. H. Oh¹⁵³, F. Ohme^{9,10}, H. Ohta⁸³, M. A. Okada¹⁵, M. Oliver¹⁰¹, P. Oppermann^{9,10}, Richard J. Oram⁷, B. O'Reilly⁷, R. G. Ormiston⁴³, L. F. Ortega³⁰, R. O'Shaughnessy⁶², S. Ossokine⁷⁶, D. J. Ottaway⁵⁷, H. Overmier⁷, B. J. Owen⁸⁵, A. E. Pace⁹⁰, G. Pagano^{20,21}, M. A. Page⁶⁶, G. Pagliaroli^{16,17}, A. Pai¹³⁰, S. A. Pai⁶⁰, J. R. Palamos⁷², O. Palashov¹⁵⁰, C. Palomba³³, H. Pan⁹¹, P. K. Panda¹⁴⁴, P. T. H. Pang^{37,94}, C. Pankow⁵⁸, F. Pannarale^{33,119}, B. C. Pant⁶⁰, F. Paoletti²¹, A. Paoli²⁹, A. Parida³, W. Parker^{7,169}, D. Pascucci^{37,46}, A. Pasqualetti²⁹, R. Passaquietti^{20,21}, D. Passuello²¹, M. Patil¹⁵⁸, B. Patricelli^{20,21}, E. Payne⁶, B. L. Pearlstone⁴⁶, T. C. Pechsiri³⁰, A. J. Pedersen⁴², M. Pedraza¹, R. Pedurand^{23,176}, A. Pele⁷, S. Penn¹⁷⁷, A. Perego^{117,118}, C. J. Perez⁴⁷, C. Péroigois³⁴, A. Perreca^{117,118}, J. Petermann¹³⁴, H. P. Pfeiffer⁷⁶, M. Phelps^{9,10}, K. S. Phukon³, O. J. Piccinni^{33,119}, M. Pichot⁶⁵, F. Piergiovanni^{63,64}, V. Pierro^{69,116}, G. Pillant²⁹, L. Pinard²³, I. M. Pinto^{69,89,116}, M. Pirello⁴⁷, M. Pitkin⁴⁶, W. Plastino^{165,166}, R. Poggiani^{20,21}, D. Y. T. Pong⁹⁴, S. Ponrathnam³, P. Popolizio²⁹, E. K. Porter²⁶, J. Powell¹⁶⁸, A. K. Prajapati¹¹¹, J. Prasad³, K. Prasai⁵¹, R. Prasanna¹⁴⁴, G. Pratten¹⁰¹, T. Prestegard²⁴, M. Principe^{69,89,116}, G. A. Prodi^{117,118}, L. Prokhorov¹³, M. Punturo⁴¹, P. Puppo³³, M. Pürrer⁷⁶, H. Qi¹⁰⁶, V. Quetschke¹⁰⁸, P. J. Quinonez³⁵, F. J. Raab⁴⁷, G. Raaijmakers^{37,142}, H. Radkins⁴⁷, N. Radulesco⁶⁵, P. Raffai¹¹⁰, S. Raja⁶⁰, C. Rajan⁶⁰

B. Rajbhandari⁸⁵, M. Rakhmanov¹⁰⁸, K. E. Ramirez¹⁰⁸, A. Ramos-Buades¹⁰¹, Javed Rana³, K. Rao⁵⁸, P. Rapagnani^{33,119}, V. Raymond¹⁰⁶, M. Razzano^{20,21}, J. Read²⁷, T. Regimbau³⁴, L. Rei⁵⁹, S. Reid²⁵, D. H. Reitze^{1,30}, P. Rettengo^{127,178}, F. Ricci^{33,119}, C. J. Richardson³⁵, J. W. Richardson¹, P. M. Ricker¹⁹, G. Riemenschneider^{127,178}, K. Riles¹³⁷, M. Rizzo⁵⁸, N. A. Robertson^{1,46}, F. Robinet²⁸, A. Rocchi³², L. Rolland³⁴, J. G. Rollins¹, V. J. Roma⁷², M. Romanelli⁷¹, J. Romano⁸⁵, R. Romano^{4,5}, C. L. Romel⁴⁷, J. H. Romie⁷, C. A. Rose²⁴, D. Rose²⁷, K. Rose¹²¹, D. Rosińska⁷⁴, S. G. Rosofsky¹⁹, M. P. Ross¹⁷⁹, S. Rowan⁴⁶, A. Rüdiger^{9,10,195}, P. Ruggi²⁹, G. Rutins¹³², K. Ryan⁴⁷, S. Sachdev⁹⁰, T. Sadecki⁴⁷, M. Sakellariadou¹⁴⁶, O. S. Salafia^{44,45,180}, L. Salconi²⁹, M. Saleem³¹, A. Samajdar³⁷, L. Sammut⁶, E. J. Sanchez¹, L. E. Sanchez¹, N. Sanchis-Gual¹⁸¹, J. R. Sanders¹⁸², K. A. Santiago³⁶, E. Santos⁶⁵, N. Sarin⁶, B. Sassolas²³, B. S. Sathyaprakash^{90,106}, O. Sauter^{34,137}, R. L. Savage⁴⁷, P. Schale⁷², M. Scheel⁴⁸, J. Scheuer⁵⁸, P. Schmidt^{13,67}, R. Schnabel¹³⁴, R. M. S. Schofield⁷², A. Schönbeck¹³⁴, E. Schreiber^{9,10}, B. W. Schulte^{9,10}, B. F. Schutz¹⁰⁶, J. Scott⁴⁶, S. M. Scott⁸, E. Seidel¹⁹, D. Sellers⁷, A. S. Sengupta¹⁸³, N. Sennett⁷⁶, D. Sentenac²⁹, V. Sequino⁵⁹, A. Sergeev¹⁵⁰, Y. Setyawati^{9,10}, D. A. Shaddock⁸, T. Shaffer⁴⁷, M. S. Shahriar⁵⁸, M. B. Shaner¹³³, A. Sharma^{16,17}, P. Sharma⁶⁰, P. Shawhan⁷⁷, H. Shen¹⁹, R. Shink¹⁸⁴, D. H. Shoemaker¹⁴, D. M. Shoemaker⁷⁸, K. Shukla¹⁴¹, S. ShyamSundar⁶⁰, K. Siellez⁷⁸, M. Sieniawska⁵⁶, D. Sigg⁴⁷, L. P. Singer⁸¹, D. Singh⁹⁰, N. Singh⁷⁴, A. Singhal^{16,33}, A. M. Sintes¹⁰¹, S. Sitmukhambetov¹⁰⁸, V. Skliris¹⁰⁶, B. J. J. Slagmolen⁸, T. J. Slaven-Blair⁶⁶, J. R. Smith²⁷, R. J. E. Smith⁶, S. Somala¹⁸⁵, E. J. Son¹⁵³, S. Soni², B. Sorazu⁴⁶, F. Sorrentino⁵⁹, T. Souradeep³, E. Sowell⁸⁵, A. P. Spencer⁴⁶, M. Spera^{53,54}, A. K. Srivastava¹¹¹, V. Srivastava⁴², K. Staats⁵⁸, C. Stachie⁶⁵, M. Standke^{9,10}, D. A. Steer²⁶, M. Steinke^{9,10}, J. Steinlechner^{46,134}, S. Steinlechner¹³⁴, D. Steinmeyer^{9,10}, S. P. Stevenson¹⁶⁸, D. Stocks⁵¹, R. Stone¹⁰⁸, D. J. Stops¹³, K. A. Strain⁴⁶, G. Stratta^{64,186}, S. E. Strigin⁶¹, A. Strunk⁴⁷, R. Sturani¹⁸⁷, A. L. Stuver¹⁸⁸, V. Sudhir¹⁴, T. Z. Summerscales¹⁸⁹, L. Sun¹, S. Sunil¹¹¹, A. Sur⁵⁶, J. Suresh⁸³, P. J. Sutton¹⁰⁶, B. L. Swinkels³⁷, M. J. Szczepańczyk³⁵, M. Tacca³⁷, S. C. Tait⁴⁶, C. Talbot⁶, D. B. Tanner³⁰, D. Tao¹, M. Tápai¹³¹, A. Tapia²⁷, J. D. Tasson⁹⁸, R. Taylor¹, R. Tenorio¹⁰¹, L. Terkowski¹³⁴, M. Thomas⁷, P. Thomas⁴⁷, S. R. Thondapu⁶⁰, K. A. Thorne⁷, E. Thrane⁶, Shubhanshu Tiwari^{117,118}, Srishti Tiwari¹³⁵, V. Tiwari¹⁰⁶, K. Toland⁴⁶, M. Tonelli^{20,21}, Z. Tornasi⁴⁶, A. Torres-Forné¹⁹⁰, C. I. Torrie¹, D. Töyrä¹³, F. Travasso^{29,41}, G. Traylor⁷, M. C. Tringali⁷⁴, A. Tripathee¹³⁷, A. Trovato²⁶, L. Trozzo^{21,191}, K. W. Tsang³⁷, M. Tse¹⁴, R. Tso⁴⁸, L. Tsukada⁸³, D. Tsuna⁸³, T. Tsutsui⁸³, D. Tuyenbayev¹⁰⁸, K. Ueno⁸³, D. Ugolini¹⁹², C. S. Unnikrishnan¹³⁵, A. L. Urban², S. A. Usman⁹³, H. Vahlbruch¹⁰, G. Vajente¹, G. Valdes², M. Valentini^{117,118}, N. van Bakel³⁷, M. van Beuzekom³⁷, J. F. J. van den Brand^{37,75}, C. Van Den Broeck^{37,193}, D. C. Vander-Hyde⁴², L. van der Schaaf³⁷, J. V. VanHeijningen⁶⁶, A. A. van Veggel⁴⁶, M. Vardaro^{53,54}, V. Varma⁴⁸, S. Vass¹, M. Vasúth⁵⁰, A. Vecchio¹³, G. Vedovato⁵⁴, J. Veitch⁴⁶, P. J. Veitch⁵⁷, K. Venkateswara¹⁷⁹, G. Venugopalan¹, D. Verkindt³⁴, F. Vetrano^{63,64}, A. Vicere^{63,64}, A. D. Viets²⁴, S. Vinciguerra¹³, D. J. Vine¹³², J.-Y. Vinet⁶⁵, S. Vitale¹⁴, T. Vo⁴², H. Vocca^{40,41}, C. Vorvick⁴⁷, S. P. Vyatchanin⁶¹, A. R. Wade¹, L. E. Wade¹²¹, M. Wade¹²¹, R. Walet³⁷, M. Walker²⁷, L. Wallace¹, S. Walsh²⁴, H. Wang¹³, J. Z. Wang¹³⁷, S. Wang¹⁹, W. H. Wang¹⁰⁸, Y. F. Wang⁹⁴, R. L. Ward⁸, Z. A. Warden³⁵, J. Warner⁴⁷, M. Was³⁴, J. Watchi¹⁰², B. Weaver⁴⁷, L.-W. Wei^{9,10}, M. Weinert^{9,10}, A. J. Weinstein¹, R. Weiss¹⁴, F. Wellmann^{9,10}, L. Wen⁶⁶, E. K. Wessel¹⁹, P. Weßels^{9,10}, J. W. Westhouse³⁵, K. Wette⁸, J. T. Whelan⁶², B. F. Whiting³⁰, C. Whittle¹⁴, D. M. Wilken^{9,10}, D. Williams⁴⁶, A. R. Williamson^{37,142}, J. L. Willis¹, B. Willke^{9,10}, W. Winkler^{9,10}, C. C. Wipf¹, H. Wittel^{9,10}, G. Woan⁴⁶, J. Woehler^{9,10}, J. K. Wofford⁶², J. L. Wright⁴⁶, D. S. Wu^{9,10}, D. M. Wysocki⁶², S. Xiao¹, R. Xu¹⁰⁹, H. Yamamoto¹, C. C. Yancey⁷⁷, L. Yang¹²⁰, Y. Yang³⁰, Z. Yang⁴³, M. J. Yap⁸, M. Yazback³⁰, D. W. Yeeles¹⁰⁶, Hang Yu¹⁴, Haocun Yu¹⁴, S. H. R. Yuen⁹⁴, A. K. Zadrożny¹⁰⁸, A. Zadrożny¹⁵⁷, M. Zanolin³⁵, T. Zelenova²⁹, J.-P. Zendri⁵⁴, M. Zevin⁵⁸, J. Zhang⁶⁶, L. Zhang¹, T. Zhang⁴⁶, C. Zhao⁶⁶, G. Zhao¹⁰², M. Zhou⁵⁸, Z. Zhou⁵⁸, X. J. Zhu⁶, A. B. Zimmerman¹⁹⁴, M. E. Zucker^{1,14}, and J. Zweizig¹

The LIGO Scientific Collaboration and the Virgo Collaboration

¹ LIGO, California Institute of Technology, Pasadena, CA 91125, USA; lsc-spokesperson@ligo.org; virgo-spokesperson@ego-gw.it

² Louisiana State University, Baton Rouge, LA 70803, USA

³ Inter-University Centre for Astronomy and Astrophysics, Pune 411007, India

⁴ Dipartimento di Farmacia, Università di Salerno, I-84084 Fisciano, Salerno, Italy

⁵ INFN, Sezione di Napoli, Complesso Universitario di Monte S. Angelo, I-80126 Napoli, Italy

⁶ OzGrav, School of Physics & Astronomy, Monash University, Clayton 3800, Victoria, Australia

⁷ LIGO Livingston Observatory, Livingston, LA 70754, USA

⁸ OzGrav, Australian National University, Canberra, Australian Capital Territory 0200, Australia

⁹ Max Planck Institute for Gravitational Physics (Albert Einstein Institute), D-30167 Hannover, Germany

¹⁰ Leibniz Universität Hannover, D-30167 Hannover, Germany

¹¹ Theoretisch-Physikalisches Institut, Friedrich-Schiller-Universität Jena, D-07743 Jena, Germany

¹² University of Cambridge, Cambridge CB2 1TN, UK

¹³ University of Birmingham, Birmingham B15 2TT, UK

¹⁴ LIGO, Massachusetts Institute of Technology, Cambridge, MA 02139, USA

¹⁵ Instituto Nacional de Pesquisas Espaciais, 12227-010 São José dos Campos, São Paulo, Brazil

¹⁶ Gran Sasso Science Institute (GSSI), I-67100 L'Aquila, Italy

¹⁷ INFN, Laboratori Nazionali del Gran Sasso, I-67100 Assergi, Italy

¹⁸ International Centre for Theoretical Sciences, Tata Institute of Fundamental Research, Bengaluru 560089, India

¹⁹ NCSA, University of Illinois at Urbana-Champaign, Urbana, IL 61801, USA

²⁰ Università di Pisa, I-56127 Pisa, Italy

²¹ INFN, Sezione di Pisa, I-56127 Pisa, Italy

²² Departamento de Astronomía y Astrofísica, Universitat de València, E-46100 Burjassot, València, Spain

²³ Laboratoire des Matériaux Avancés (LMA), CNRS/IN2P3, F-69622 Villeurbanne, France

²⁴ University of Wisconsin-Milwaukee, Milwaukee, WI 53201, USA

²⁵ SUPA, University of Strathclyde, Glasgow G1 1XQ, UK

- ²⁶ APC, AstroParticule et Cosmologie, Université Paris Diderot, CNRS/IN2P3, CEA/Irfu, Observatoire de Paris, Sorbonne Paris Cité, F-75205 Paris Cedex 13, France
- ²⁷ California State University Fullerton, Fullerton, CA 92831, USA
- ²⁸ LAL, Université Paris-Sud, CNRS/IN2P3, Université Paris-Saclay, F-91898 Orsay, France
- ²⁹ European Gravitational Observatory (EGO), I-56021 Cascina, Pisa, Italy
- ³⁰ University of Florida, Gainesville, FL 32611, USA
- ³¹ Chennai Mathematical Institute, Chennai 603103, India
- ³² INFN, Sezione di Roma Tor Vergata, I-00133 Roma, Italy
- ³³ INFN, Sezione di Roma, I-00185 Roma, Italy
- ³⁴ Laboratoire d'Annecy de Physique des Particules (LAPP), Université Grenoble Alpes, Université Savoie Mont Blanc, CNRS/IN2P3, F-74941 Annecy, France
- ³⁵ Embry-Riddle Aeronautical University, Prescott, AZ 86301, USA
- ³⁶ Montclair State University, Montclair, NJ 07043, USA
- ³⁷ Nikhef, Science Park 105, 1098 XG Amsterdam, The Netherlands
- ³⁸ Korea Institute of Science and Technology Information, Daejeon 34141, Republic of Korea
- ³⁹ West Virginia University, Morgantown, WV 26506, USA
- ⁴⁰ Università di Perugia, I-06123 Perugia, Italy
- ⁴¹ INFN, Sezione di Perugia, I-06123 Perugia, Italy
- ⁴² Syracuse University, Syracuse, NY 13244, USA
- ⁴³ University of Minnesota, Minneapolis, MN 55455, USA
- ⁴⁴ Università degli Studi di Milano-Bicocca, I-20126 Milano, Italy
- ⁴⁵ INFN, Sezione di Milano-Bicocca, I-20126 Milano, Italy
- ⁴⁶ SUPA, University of Glasgow, Glasgow G12 8QQ, UK
- ⁴⁷ LIGO Hanford Observatory, Richland, WA 99352, USA
- ⁴⁸ Caltech CaRT, Pasadena, CA 91125, USA
- ⁴⁹ Dipartimento di Medicina, Chirurgia e Odontoiatria "Scuola Medica Salernitana," Università di Salerno, I-84081 Baronissi, Salerno, Italy
- ⁵⁰ Wigner RCP, RMKI, H-1121 Budapest, Konkoly Thege Miklós út 29-33, Hungary
- ⁵¹ Stanford University, Stanford, CA 94305, USA
- ⁵² Università di Camerino, Dipartimento di Fisica, I-62032 Camerino, Italy
- ⁵³ Università di Padova, Dipartimento di Fisica e Astronomia, I-35131 Padova, Italy
- ⁵⁴ INFN, Sezione di Padova, I-35131 Padova, Italy
- ⁵⁵ Montana State University, Bozeman, MT 59717, USA
- ⁵⁶ Nicolaus Copernicus Astronomical Center, Polish Academy of Sciences, 00-716, Warsaw, Poland
- ⁵⁷ OzGrav, University of Adelaide, Adelaide, South Australia 5005, Australia
- ⁵⁸ Center for Interdisciplinary Exploration & Research in Astrophysics (CIERA), Northwestern University, Evanston, IL 60208, USA
- ⁵⁹ INFN, Sezione di Genova, I-16146 Genova, Italy
- ⁶⁰ RRCAT, Indore, Madhya Pradesh 452013, India
- ⁶¹ Faculty of Physics, Lomonosov Moscow State University, Moscow 119991, Russia
- ⁶² Rochester Institute of Technology, Rochester, NY 14623, USA
- ⁶³ Università degli Studi di Urbino "Carlo Bo," I-61029 Urbino, Italy
- ⁶⁴ INFN, Sezione di Firenze, I-50019 Sesto Fiorentino, Firenze, Italy
- ⁶⁵ Artemis, Université Côte d'Azur, Observatoire Côte d'Azur, CNRS, CS 34229, F-06304 Nice Cedex 4, France
- ⁶⁶ OzGrav, University of Western Australia, Crawley, Western Australia 6009, Australia
- ⁶⁷ Department of Astrophysics/IMAPP, Radboud University Nijmegen, P.O. Box 9010, 6500 GL Nijmegen, The Netherlands
- ⁶⁸ Dipartimento di Fisica "E.R. Caianiello," Università di Salerno, I-84084 Fisciano, Salerno, Italy
- ⁶⁹ INFN, Sezione di Napoli, Gruppo Collegato di Salerno, Complesso Universitario di Monte S. Angelo, I-80126 Napoli, Italy
- ⁷⁰ Physik-Institut, University of Zurich, Winterthurerstrasse 190, 8057 Zurich, Switzerland
- ⁷¹ Univ Rennes, CNRS, Institut FOTON—UMR6082, F-3500 Rennes, France
- ⁷² University of Oregon, Eugene, OR 97403, USA
- ⁷³ Laboratoire Kastler Brossel, Sorbonne Université, CNRS, ENS-Université PSL, Collège de France, F-75005 Paris, France
- ⁷⁴ Astronomical Observatory Warsaw University, 00-478 Warsaw, Poland
- ⁷⁵ VU University Amsterdam, 1081 HV Amsterdam, The Netherlands
- ⁷⁶ Max Planck Institute for Gravitational Physics (Albert Einstein Institute), D-14476 Potsdam-Golm, Germany
- ⁷⁷ University of Maryland, College Park, MD 20742, USA
- ⁷⁸ School of Physics, Georgia Institute of Technology, Atlanta, GA 30332, USA
- ⁷⁹ Université de Lyon, Université Claude Bernard Lyon 1, CNRS, Institut Lumière Matière, F-69622 Villeurbanne, France
- ⁸⁰ Università di Napoli "Federico II," Complesso Universitario di Monte S. Angelo, I-80126 Napoli, Italy
- ⁸¹ NASA Goddard Space Flight Center, Greenbelt, MD 20771, USA
- ⁸² Dipartimento di Fisica, Università degli Studi di Genova, I-16146 Genova, Italy
- ⁸³ RESCEU, University of Tokyo, Tokyo, 113-0033, Japan
- ⁸⁴ Tsinghua University, Beijing 100084, People's Republic of China
- ⁸⁵ Texas Tech University, Lubbock, TX 79409, USA
- ⁸⁶ Università di Roma Tor Vergata, I-00133 Roma, Italy
- ⁸⁷ The University of Mississippi, University, MS 38677, USA
- ⁸⁸ Missouri University of Science and Technology, Rolla, MO 65409, USA
- ⁸⁹ Museo Storico della Fisica e Centro Studi e Ricerche "Enrico Fermi," I-00184 Roma, Italy
- ⁹⁰ The Pennsylvania State University, University Park, PA 16802, USA
- ⁹¹ National Tsing Hua University, Hsinchu City, 30013 Taiwan, People's Republic of China
- ⁹² Charles Sturt University, Wagga Wagga, New South Wales 2678, Australia
- ⁹³ University of Chicago, Chicago, IL 60637, USA
- ⁹⁴ The Chinese University of Hong Kong, Shatin, NT, Hong Kong
- ⁹⁵ Dipartimento di Ingegneria Industriale (DIIN), Università di Salerno, I-84084 Fisciano, Salerno, Italy
- ⁹⁶ Seoul National University, Seoul 08826, Republic of Korea
- ⁹⁷ Pusan National University, Busan 46241, Republic of Korea
- ⁹⁸ Carleton College, Northfield, MN 55057, USA
- ⁹⁹ INAF, Osservatorio Astronomico di Padova, I-35122 Padova, Italy
- ¹⁰⁰ OzGrav, University of Melbourne, Parkville, Victoria 3010, Australia

- ¹⁰¹ Universitat de les Illes Balears, IAC3—IEEC, E-07122 Palma de Mallorca, Spain
- ¹⁰² Université Libre de Bruxelles, Brussels B-1050, Belgium
- ¹⁰³ Sonoma State University, Rohnert Park, CA 94928, USA
- ¹⁰⁴ Departamento de Matemáticas, Universitat de València, E-46100 Burjassot, València, Spain
- ¹⁰⁵ Columbia University, New York, NY 10027, USA
- ¹⁰⁶ Cardiff University, Cardiff CF24 3AA, UK
- ¹⁰⁷ University of Rhode Island, Kingston, RI 02881, USA
- ¹⁰⁸ The University of Texas Rio Grande Valley, Brownsville, TX 78520, USA
- ¹⁰⁹ Bellevue College, Bellevue, WA 98007, USA
- ¹¹⁰ MTA-ELTE Astrophysics Research Group, Institute of Physics, Eötvös University, Budapest 1117, Hungary
- ¹¹¹ Institute for Plasma Research, Bhat, Gandhinagar 382428, India
- ¹¹² The University of Sheffield, Sheffield S10 2TN, UK
- ¹¹³ IGFAE, Campus Sur, Universidade de Santiago de Compostela, E-15782, Spain
- ¹¹⁴ Dipartimento di Scienze Matematiche, Fisiche e Informatiche, Università di Parma, I-43124 Parma, Italy
- ¹¹⁵ INFN, Sezione di Milano Bicocca, Gruppo Collegato di Parma, I-43124 Parma, Italy
- ¹¹⁶ Dipartimento di Ingegneria, Università del Sannio, I-82100 Benevento, Italy
- ¹¹⁷ Università di Trento, Dipartimento di Fisica, I-38123 Povo, Trento, Italy
- ¹¹⁸ INFN, Trento Institute for Fundamental Physics and Applications, I-38123 Povo, Trento, Italy
- ¹¹⁹ Università di Roma “La Sapienza,” I-00185 Roma, Italy
- ¹²⁰ Colorado State University, Fort Collins, CO 80523, USA
- ¹²¹ Kenyon College, Gambier, OH 43022, USA
- ¹²² Christopher Newport University, Newport News, VA 23606, USA
- ¹²³ CNR-SPIN, c/o Università di Salerno, I-84084 Fisciano, Salerno, Italy
- ¹²⁴ Scuola di Ingegneria, Università della Basilicata, I-85100 Potenza, Italy
- ¹²⁵ National Astronomical Observatory of Japan, 2-21-1 Osawa, Mitaka, Tokyo 181-8588, Japan
- ¹²⁶ Observatori Astronòmic, Universitat de València, E-46980 Paterna, València, Spain
- ¹²⁷ INFN Sezione di Torino, I-10125 Torino, Italy
- ¹²⁸ School of Mathematics, University of Edinburgh, Edinburgh EH9 3FD, UK
- ¹²⁹ Institute Of Advanced Research, Gandhinagar 382426, India
- ¹³⁰ Indian Institute of Technology Bombay, Powai, Mumbai 400 076, India
- ¹³¹ University of Szeged, Dóm tér 9, Szeged 6720, Hungary
- ¹³² SUPA, University of the West of Scotland, Paisley PA1 2BE, UK
- ¹³³ California State University, Los Angeles, 5151 State University Dr, Los Angeles, CA 90032, USA
- ¹³⁴ Universität Hamburg, D-22761 Hamburg, Germany
- ¹³⁵ Tata Institute of Fundamental Research, Mumbai 400005, India
- ¹³⁶ INAF, Osservatorio Astronomico di Capodimonte, I-80131 Napoli, Italy
- ¹³⁷ University of Michigan, Ann Arbor, MI 48109, USA
- ¹³⁸ Washington State University, Pullman, WA 99164, USA
- ¹³⁹ American University, Washington, D.C. 20016, USA
- ¹⁴⁰ University of Portsmouth, Portsmouth, PO1 3FX, UK
- ¹⁴¹ University of California, Berkeley, CA 94720, USA
- ¹⁴² GRAPPA, Anton Pannekoek Institute for Astronomy and Institute for High-Energy Physics, University of Amsterdam, Science Park 904, 1098 XH Amsterdam, The Netherlands
- ¹⁴³ Delta Institute for Theoretical Physics, Science Park 904, 1090 GL Amsterdam, The Netherlands
- ¹⁴⁴ Directorate of Construction, Services & Estate Management, Mumbai 400094, India
- ¹⁴⁵ University of Białystok, 15-424 Białystok, Poland
- ¹⁴⁶ King’s College London, University of London, London WC2R 2LS, UK
- ¹⁴⁷ University of Southampton, Southampton SO17 1BJ, UK
- ¹⁴⁸ Institut de Física d’Altes Energies (IFAE), Barcelona Institute of Science and Technology, and ICREA, E-08193 Barcelona, Spain
- ¹⁴⁹ University of Washington Bothell, Bothell, WA 98011, USA
- ¹⁵⁰ Institute of Applied Physics, Nizhny Novgorod, 603950, Russia
- ¹⁵¹ Ewha Womans University, Seoul 03760, Republic of Korea
- ¹⁵² Inje University Gimhae, South Gyeongsang 50834, Republic of Korea
- ¹⁵³ National Institute for Mathematical Sciences, Daejeon 34047, Republic of Korea
- ¹⁵⁴ Ulsan National Institute of Science and Technology, Ulsan 44919, Republic of Korea
- ¹⁵⁵ Maastricht University, P.O. Box 616, 6200 MD Maastricht, The Netherlands
- ¹⁵⁶ Bard College, 30 Campus Rd, Annandale-On-Hudson, NY 12504, USA
- ¹⁵⁷ NCBJ, 05-400 Świerk-Otwock, Poland
- ¹⁵⁸ Institute of Mathematics, Polish Academy of Sciences, 00656 Warsaw, Poland
- ¹⁵⁹ Cornell University, Ithaca, NY 14850, USA
- ¹⁶⁰ Hillsdale College, Hillsdale, MI 49242, USA
- ¹⁶¹ Hanyang University, Seoul 04763, Republic of Korea
- ¹⁶² Korea Astronomy and Space Science Institute, Daejeon 34055, Republic of Korea
- ¹⁶³ Institute for High-Energy Physics, University of Amsterdam, Science Park 904, 1098 XH Amsterdam, The Netherlands
- ¹⁶⁴ NASA Marshall Space Flight Center, Huntsville, AL 35811, USA
- ¹⁶⁵ Dipartimento di Matematica e Fisica, Università degli Studi Roma Tre, I-00146 Roma, Italy
- ¹⁶⁶ INFN, Sezione di Roma Tre, I-00146 Roma, Italy
- ¹⁶⁷ ESPCI, CNRS, F-75005 Paris, France
- ¹⁶⁸ OzGrav, Swinburne University of Technology, Hawthorn VIC 3122, Australia
- ¹⁶⁹ Southern University and A&M College, Baton Rouge, LA 70813, USA
- ¹⁷⁰ Centre Scientifique de Monaco, 8 quai Antoine 1er, MC-98000, Monaco
- ¹⁷¹ Indian Institute of Technology Madras, Chennai 600036, India
- ¹⁷² Institut des Hautes Etudes Scientifiques, F-91440 Bures-sur-Yvette, France
- ¹⁷³ IISER-Kolkata, Mohanpur, West Bengal 741252, India
- ¹⁷⁴ Institut für Kernphysik, Theoriezentrum, 64289 Darmstadt, Germany
- ¹⁷⁵ Whitman College, 345 Boyer Avenue, Walla Walla, WA 99362, USA

- ¹⁷⁶ Université de Lyon, F-69361 Lyon, France
¹⁷⁷ Hobart and William Smith Colleges, Geneva, NY 14456, USA
¹⁷⁸ Dipartimento di Fisica, Università degli Studi di Torino, I-10125 Torino, Italy
¹⁷⁹ University of Washington, Seattle, WA 98195, USA
¹⁸⁰ INAF, Osservatorio Astronomico di Brera sede di Merate, I-23807 Merate, Lecco, Italy
¹⁸¹ Centro de Astrofísica e Gravitação (CENTRA), Departamento de Física, Instituto Superior Técnico, Universidade de Lisboa, 1049-001 Lisboa, Portugal
¹⁸² Marquette University, 11420 W. Clybourn Street, Milwaukee, WI 53233, USA
¹⁸³ Indian Institute of Technology, Gandhinagar Ahmedabad Gujarat 382424, India
¹⁸⁴ Université de Montréal/Polytechnique, Montreal, Quebec H3T 1J4, Canada
¹⁸⁵ Indian Institute of Technology Hyderabad, Sangareddy, Khandi, Telangana 502285, India
¹⁸⁶ INAF, Osservatorio di Astrofisica e Scienza dello Spazio, I-40129 Bologna, Italy
¹⁸⁷ International Institute of Physics, Universidade Federal do Rio Grande do Norte, Natal RN 59078-970, Brazil
¹⁸⁸ Villanova University, 800 Lancaster Ave, Villanova, PA 19085, USA
¹⁸⁹ Andrews University, Berrien Springs, MI 49104, USA
¹⁹⁰ Max Planck Institute for Gravitationalphysik (Albert Einstein Institute), D-14476 Potsdam-Golm, Germany
¹⁹¹ Università di Siena, I-53100 Siena, Italy
¹⁹² Trinity University, San Antonio, TX 78212, USA
¹⁹³ Van Swinderen Institute for Particle Physics and Gravity, University of Groningen, Nijenborgh 4, 9747 AG Groningen, The Netherlands
¹⁹⁴ Department of Physics, University of Texas, Austin, TX 78712, USA

Received 2019 August 21; revised 2020 November 7; accepted 2020 December 11; published 2021 March 19

Abstract

This paper presents the gravitational-wave measurement of the Hubble constant (H_0) using the detections from the first and second observing runs of the Advanced LIGO and Virgo detector network. The presence of the transient electromagnetic counterpart of the binary neutron star GW170817 led to the first standard-siren measurement of H_0 . Here we additionally use binary black hole detections in conjunction with galaxy catalogs and report a joint measurement. Our updated measurement is $H_0 = 69^{+16}_{-8} \text{ km s}^{-1} \text{ Mpc}^{-1}$ (68.3% of the highest density posterior interval with a flat-in-log prior) which is an improvement by a factor of 1.04 (about 4%) over the GW170817-only value of $69^{+17}_{-8} \text{ km s}^{-1} \text{ Mpc}^{-1}$. A significant additional contribution currently comes from GW170814, a loud and well-localized detection from a part of the sky thoroughly covered by the Dark Energy Survey. With numerous detections anticipated over the upcoming years, an exhaustive understanding of other systematic effects are also going to become increasingly important. These results establish the path to cosmology using gravitational-wave observations with and without transient electromagnetic counterparts.

Key words: Gravitational wave astronomy – Hubble constant

1. Introduction

Gravitational waves (GWs) from compact binary coalescences allow for the direct measurement of the luminosity distance to their source. This makes them standard-distance indicators, and in conjunction with an identified host galaxy or a set of possible host galaxies, they can be used as standard sirens to construct a redshift-distance relationship and measure cosmological parameters like the Hubble constant (H_0 ; Schutz 1986; Holz & Hughes 2005; MacLeod & Hogan 2008; Nissanke et al. 2010; Sathyaprakash et al. 2010). The GW signature from the binary neutron star (BNS) merger GW170817, along with its coincident electromagnetic (EM) transient associated with the host galaxy NGC4993, led to a first standard-siren measurement of H_0 (Abbott et al. 2017a). This measurement is independent of other state-of-the-art measurements of H_0 , and in particular, independent of the cosmic distance ladder used to calibrate standardizable sources like SNe Ia (Type Ia supernovae). The importance of an independent measurement of H_0 is worth highlighting. With the Planck 2018 data release (Planck Collaboration et al. 2020), and the recalibration of supernovae using Large Magellanic Cloud Cepheids (Riess et al. 2019), the tension between early

universe measurements of H_0 from Planck and local measurements from the Supernovae H0 for the Equation of State (SHOES) project has risen to the 4.4σ level. Independent measurements using cosmological baryon acoustic oscillations to calibrate SNe Ia via the inverse distance ladder (Macaulay et al. 2019) and gravitational lensing of quasars in the nearby universe (H0LiCOW Collaboration, Birrer et al. 2019) favor to some degree the early universe Planck and the local SHOES measurements, respectively. A complementary measurement of H_0 from the multimessenger GW astronomy sector would help clarify whether the current tension is a statistical anomaly or evidence for new physics beyond the Lambda cold dark matter (Λ CDM) model of cosmology.¹⁹⁶

The GW standard-siren measurement in Abbott et al. (2017a) is broadly consistent with other measurements. By combining information from multiple detections, one can improve the accuracy reaching about 1% with $\mathcal{O}(100)$ detections in the coming years (Dalal et al. 2006; Nissanke et al. 2013; Chen et al. 2018; Vitale & Chen 2018; Feeney et al. 2019; Mortlock et al. 2019).

An unambiguous identification of the host galaxy is unlikely for all BNS detections; only a crude estimate of the sky position may be available. Moreover there are sources such as

¹⁹⁵ Deceased, 2018 July.

¹⁹⁶ Cosmological parameters can potentially be inferred from GW observations alone by estimating the redshift using the known physics of neutron stars (Messenger & Read 2012) or their astrophysical mass distribution (Finn 1994; Taylor & Gair 2012); however these methods are not expected to find an application in context of the current generation of advanced ground-based detectors. Prospects of GW cosmology using robust astrophysical features of black hole mass distributions have recently been explored in Farr et al. (2019).

binary black hole (BBH) mergers with no expected EM counterparts. Even in the absence of an EM counterpart, the method outlined in Schutz (1986) can be used: with a set of potential host galaxies identified in a galaxy catalog for each detection, one can build up information by a process of statistical cross-correlation. The method was demonstrated on a set of simulations in Del Pozzo (2012), where a 5% estimate on H_0 was obtained from $\mathcal{O}(100)$ detections in an idealized situation of nearby events and complete galaxy catalogs; similar results with projections for third-generation detectors have been obtained in Nair et al. (2018). It has further been shown in Chen et al. (2018) that the main benefit of the galaxy-catalog method would be for the case of multiple well-localized sources.

An understanding of GW selection effects (Abbott et al. 2017a; Chen et al. 2018; Mandel et al. 2019; Vitale et al. 2020) and features of galaxy catalogs, such as their incompleteness and measurement uncertainties, is necessary for an accurate measurement of H_0 . Prescriptions to handle incomplete galaxy catalogs have been outlined in Chen et al. (2018), Fishbach et al. (2019), and Gray et al. (2020), and an extensive study of selection effects including galaxy catalog completeness has been performed in Gray et al. (2020). The simulations in Gray et al. (2020) demonstrate that the current method is able to handle galaxy catalog completeness down to $\sim 25\%$ for $\mathcal{O}(100)$ detections in the nearby universe (luminosity distance $d_L \lesssim 115$ Mpc) with idealized galaxy catalogs, without introducing additional systematic features. The galaxy-catalog method was used in Fishbach et al. (2019) to infer H_0 from GW170817 without its optical counterpart. An estimate of H_0 from GW170814 and the photometric redshift catalog from the Dark Energy Survey (DES) Year 3 data was also obtained in Soares-Santos et al. (2019).

In this paper we report the first joint GW estimate of H_0 from detections during O1 and O2, the first and second observing runs of the Advanced LIGO and Virgo detector network. For our final result, along with the BNS GW170817, we choose the six O1 and O2 BBH detections, which satisfy our selection criterion of a network signal-to-noise ratio (S/N) > 12 in at least one search pipeline for GW detections. The detections for which we have significant galaxy catalog support are GW150914, GW151226, GW170608, and GW170814. For these events, we expect the inferred H_0 posteriors to be driven by the additional EM information. The two remaining BBHs that satisfy the selection criterion, GW170104 and GW170809, need to be retained in the analysis for consistency with the assumed population model. These events for which a significant fraction of potential host galaxies are missing in the associated galaxy catalog, can also potentially contribute to the H_0 measurement, since there is information about cosmology present in the observed source distribution (Taylor et al. 2012; Taylor & Gair 2012; Farr et al. 2019). The distribution of the observed source parameters, including the observed luminosity distance distribution, is driven by H_0 in addition to the intrinsic astrophysical source distributions. With a known underlying astrophysical distribution of sources, H_0 would be measurable solely from the observed distance distribution of BBH detections (Chen & Holz 2014). This latter contribution is not expected to provide significant information at this stage given how uncertain the inferred astrophysical distribution parameters such as the power-law index of the binary mass distribution, or the index characterizing the evolution of the binary merger rate with redshift are, even when H_0 is held fixed

(Abbott et al. 2019a). In an ideal situation, one should jointly estimate these astrophysical population parameters along with H_0 . We choose to fix the astrophysical population to a fiducial distribution instead, and perform our analysis with different choices for the mass distribution and binary merger rate evolution with redshift in order to quantify possible systematic effects resulting from this assumption. We set aside a more thorough treatment involving the marginalization over the unknown astrophysical distribution for future work.

The main result of our analysis—a posterior distribution on H_0 —is dominated by the contribution from GW170817 with its optical counterpart, with a modest improvement from the inclusion of the O1 and O2 BBH. These results, possibly refined and marginalized over the aforementioned assumptions, can be used as a prior for future GW estimates of H_0 . The analysis performed in this paper thus serves as a precursor of future analyses for the third and subsequent observing runs of the advanced detector network.

The rest of this paper is arranged as follows. We describe our method in Section 2. We summarize the GW detections we use in our analysis and the corresponding EM data in Section 3. Our main results are presented in Section 4, with a more detailed discussion and a study of possible systematic effects in Section 5. We conclude in Section 6 and highlight some future directions and prospects.

Throughout this paper we assume a Λ CDM cosmology and use the best-fit Planck 2015 values of $\Omega_m = 0.308$ and $\Omega_\Lambda = 0.692$, respectively for the fractional matter and dark energy densities in the present epoch (Planck Collaboration 2016). Although these parameters enter the redshift-distance relationship central to the method for Bayesian inference of H_0 , we have verified that our results are robust with regards to a variation of their values within the current measurement uncertainties.

2. Method

We follow and apply the Bayesian analysis described in Gray et al. (2020) to compute the posterior probability density on H_0 , given the set $\{D_{\text{GW}}\}$ of N_{det} detections and the associated GW data $\{x_{\text{GW}}\}$:

$$p(H_0 | \{x_{\text{GW}}\}, \{D_{\text{GW}}\}) \propto p(H_0) p(N_{\text{det}} | H_0) \prod_i^{N_{\text{det}}} p(x_{\text{GW}i} | D_{\text{GW}i}, H_0). \quad (1)$$

Here, $D_{\text{GW}i}$ indicates that the event i was detected as a GW, $p(H_0)$ is the prior on H_0 , and the term $p(N_{\text{det}} | H_0)$ is the likelihood of detecting N_{det} events over the time of observation with the associated detector configuration for the given value of H_0 . The number of detected events is some fraction of the total number of sources N_s , and this fraction depends on H_0 ; thus, $N_{\text{det}} = f_{\text{det}}(H_0) N_s$. If the intrinsic astrophysical merger rate, R , which N_s is proportional to,¹⁹⁷ is marginalized over with a prior $p(R) \propto R^{-1}$, then $p(N_{\text{det}} | H_0) = \int p(N_{\text{det}} | H_0, R) p(R) dR$ is independent of $f_{\text{det}}(H_0)$, and thus loses its dependence on H_0 (see, e.g., Fishbach et al. 2018). For simplicity, we make this approximation throughout our analysis. The final term

¹⁹⁷ The astrophysical merger rate is defined as $R \equiv \partial N_s / (\partial V \partial T)$, where N_s is the number of sources as in the text, V the comoving sensitive volume, and T the time of observation or survey.

factorizes into the individual likelihoods for each detection. In the following, we write out the expressions for a single GW event i , omitting the subscript i for brevity of notation:

$$p(x_{\text{GW}}|D_{\text{GW}}, H_0) = \frac{p(D_{\text{GW}}|x_{\text{GW}}, H_0)p(x_{\text{GW}}|H_0)}{p(D_{\text{GW}}|H_0)}. \quad (2)$$

The denominator, $p(D_{\text{GW}}|H_0)$, is evaluated as an integral over all possible x_{GW} (Abbott et al. 2017a; Chen et al. 2018; Mandel et al. 2019):

$$p(D_{\text{GW}}|H_0) = \int p(D_{\text{GW}}|x_{\text{GW}}, H_0)p(x_{\text{GW}}|H_0)dx_{\text{GW}}, \quad (3)$$

where $p(D_{\text{GW}}|x_{\text{GW}}, H_0) = 1$ in the case where the S/N of x_{GW} passes some detection threshold, and 0 in the case where it does not.

2.1. The EM Counterpart Case

In the presence of an EM counterpart, there is additional information in the EM data, x_{EM} , which appears as an EM likelihood term. Together with this, there is an underlying assumption that there has been an EM detection; we denote this assumption as D_{EM} . Thus, for a single event with an EM counterpart,

$$\begin{aligned} & p(x_{\text{GW}}, x_{\text{EM}}|D_{\text{GW}}, D_{\text{EM}}, H_0) \\ &= \frac{p(x_{\text{GW}}|H_0)p(x_{\text{EM}}|H_0)}{p(D_{\text{EM}}|D_{\text{GW}}, H_0)p(D_{\text{GW}}|H_0)}. \end{aligned} \quad (4)$$

We assume that the detectability of an EM counterpart is dependent on luminosity distance (as opposed to redshift) because it is flux limited. As GW detectability is also a function of luminosity distance, we expect $p(D_{\text{EM}}|D_{\text{GW}}, H_0)$ to be a constant that does not depend on H_0 . This leads to

$$p(x_{\text{GW}}, x_{\text{EM}}|D_{\text{GW}}, D_{\text{EM}}, H_0) \approx \frac{p(x_{\text{GW}}|H_0)p(x_{\text{EM}}|H_0)}{p(D_{\text{GW}}|H_0)}. \quad (5)$$

2.2. The Galaxy-catalog Case

In the absence of an EM counterpart, the analogous data comes from galaxy catalogs that provide a set of galaxies and their associated sky locations, redshifts, and apparent magnitudes. As we are in the regime where the detectability of GW sources extends beyond the distance to which current catalogs are complete, the possibility that the GW host galaxy is not contained in the catalog, because it is too faint, has to be taken into account. This is done by marginalizing over the cases where the host is in the catalog (denoted G), and where it is not (denoted \bar{G}):

$$\begin{aligned} p(x_{\text{GW}}|D_{\text{GW}}, H_0) &= p(x_{\text{GW}}|G, D_{\text{GW}}, H_0)p(G|D_{\text{GW}}, H_0) \\ &+ p(x_{\text{GW}}|\bar{G}, D_{\text{GW}}, H_0)p(\bar{G}|D_{\text{GW}}, H_0). \end{aligned} \quad (6)$$

In the case where the host galaxy is in the catalog, the EM data enters in the form of information available in the galaxy catalog, as also in Fishbach et al. (2019) and Soares-Santos et al. (2019). This assumption is included in our conditioning on G . The EM information is used to modify our priors on galaxy redshift, sky location, and (apparent) magnitude, which are common among all GW events using the same catalog. This

differs from the counterpart case where the EM data enters the expression as a likelihood term, x_{EM} , a transient which is informative for only one GW event. In the case where the host galaxy is not in the catalog, the complementary condition \bar{G} implies that we include the information about the limitations of the EM survey. Following Gray et al. (2020), we model the galaxy catalog as having an apparent magnitude threshold, m_{th} , since galaxy catalogs are flux limited. This magnitude threshold, alongside the intrinsic (absolute) brightness of a galaxy and its luminosity distance, determines the probability that the galaxy is inside or outside the galaxy catalog.

The formalism which we adopt from Gray et al. (2020) is closely analogous to the method described in Chen et al. (2018) and Fishbach et al. (2019). The in-catalog and out-of-catalog terms in Equation (6) above correspond to the two terms in Equation (3) of Fishbach et al. (2019). However, the methods start formally differing in the way that the (in)completeness of the galaxy catalog is treated. In the current formalism from Gray et al. (2020), the (in)completeness of the galaxy catalog follows naturally from the parameters of the underlying EM survey(s). The assumption that a galaxy catalog can be modeled by a single m_{th} in each direction of the sky is an idealization. However, this can in the future be extended to include nontrivial selection functions modeling the optical sensitivity of the telescope instead of a sharp cutoff at m_{th} , and to composite catalogs coming from multiple surveys.

The quantities appearing on the right in Equation (6) can be written out explicitly as follows:

$$\begin{aligned} & p(x_{\text{GW}}|G, D_{\text{GW}}, H_0) \\ &= \frac{\sum_{j=1}^{N_{\text{gal}}} \int p(x_{\text{GW}}|z_j, \Omega_j, H_0)p(s|M(z_j, m_j, H_0))p(z_j)dz_j}{\sum_{j=1}^{N_{\text{gal}}} \int p(D_{\text{GW}}|z_j, \Omega_j, H_0)p(s|M(z_j, m_j, H_0))p(z_j)dz_j}. \end{aligned} \quad (7)$$

Here, N_{gal} is the total number of galaxies in the galaxy catalog, Ω_j and m_j are respectively the sky coordinates and apparent magnitude for galaxy j , and $p(z_j)$ is a distribution representing the redshift of galaxy j . This quantity, $p(z_j)$, which enters as a prior for our analysis, is the posterior distribution on the galaxy redshift obtained following analysis of EM data; details of the profiles chosen for $p(z_j)$ are deferred until Section 3.4.1. The quantity $M(z_j, m_j, H_0)$ is the absolute magnitude (for the given H_0), and $p(s|M(z_j, m_j, H_0))$ is the probability of a galaxy with these parameters to host a GW source during the observation time, relative to other galaxies. Formally, s is the statement that a GW has been *sourced* or *emitted* (as opposed to being *detected*); the previous expressions are all implicitly conditioned on the assumption of s . In writing $p(s|M)$, we make the approximation that the probability of a galaxy hosting a source depends only on the intrinsic luminosity of the galaxy, and not on its other parameters or on the properties of the GW source. In essence, this term allows for weighting galaxies by their luminosities $L(M_j(H_0))$ as

$$p(s|M(z_j, m_j, H_0)) \propto \begin{cases} \text{constant} & \text{if unweighted} \\ L(M_j(H_0)) & \text{if luminosity weighted.} \end{cases} \quad (8)$$

The likelihood when the host galaxy is not in the catalog, $p(x_{\text{GW}}|\bar{G}, D_{\text{GW}}, H_0)$, is a ratio of marginalized integrals:

$$p(x_{\text{GW}}|\bar{G}, D_{\text{GW}}, H_0) = \frac{\iiint_{z(m_{\text{th}}, M, H_0)}^{\infty} p(x_{\text{GW}}|z, \Omega, H_0) p(z) p(\Omega) p(M|H_0) p(s|M) dz d\Omega dM}{\iiint_{z(m_{\text{th}}, M, H_0)}^{\infty} p(D_{\text{GW}}|z, \Omega, H_0) p(z) p(\Omega) p(M|H_0) p(s|M) dz d\Omega dM}. \quad (9)$$

Here, the fact that the terms are conditioned on \bar{G} is incorporated into the redshift limits as a function of the apparent magnitude threshold m_{th} of the galaxy catalog. Finally, the prior probabilities that a given GW detection has or does not have support in the galaxy catalog are, respectively,

$$p(G|D_{\text{GW}}, H_0) = \frac{\iiint_0^{z(m_{\text{th}}, M, H_0)} p(D_{\text{GW}}|z, \Omega, H_0) p(z) p(\Omega) p(M|H_0) p(s|M) dz d\Omega dM}{\iiint_0^{\infty} p(D_{\text{GW}}|z, \Omega, H_0) p(z) p(\Omega) p(M|H_0) p(s|M) dz d\Omega dM},$$

and $p(\bar{G}|D_{\text{GW}}, H_0) = 1 - p(G|D_{\text{GW}}, H_0)$. (10)

In Equations (9) and (10), $p(z)$ is the prior on the redshift of host galaxies of GW events, taken to be of the form

$$p(z) \propto \frac{1}{1+z} \frac{dV_c(z)}{dz} R(z). \quad (11)$$

Here, $V_c(z)$ is the comoving volume as a function of redshift and the factor $(1+z)^{-1}$ converts the merger rate from the source frame to the detector frame. The merger rate density may in general be a function of redshift; however, we set $R(z) = \text{constant}$ throughout (other than in Section 5, where we consider an alternative redshift-dependent rate model). The prior on the GW sky location $p(\Omega)$ is taken to be uniform across the sky. The term $p(M|H_0)$ is the prior on absolute magnitudes for all the galaxies in the universe (not just those inside the galaxy catalog), which we set to follow the Schechter luminosity function:

$$p(M|H_0) \propto 10^{-0.4(\alpha+1)(M-M^*(H_0))} \exp[-10^{-0.4(M-M^*(H_0))}]. \quad (12)$$

Following Gehrels et al. (2016), we use B -band luminosity function parameters $\alpha = -1.07$ for the slope of the Schechter function and $M^*(H_0) = -19.7 + 5 \log_{10} h$ for its characteristic absolute magnitude (with $h \equiv H_0/100 \text{ km s}^{-1} \text{ Mpc}^{-1}$) throughout, unless otherwise specified.¹⁹⁸ For the upper limits of integration over M , we choose the magnitude of the dimmest galaxies to be $-12.2 + 5 \log_{10} h$. The integrals are not sensitive to the choice of their lower limits, i.e., the magnitudes of the brightest galaxies. More complex models for $p(M|H_0)$ can be used; in fact, we expect the luminosity distribution of galaxies to also evolve with redshift (Caditz & Petrosian 1989), as well as to depend on galaxy type and color (Madgwick et al. 2002). While the consideration of such dependence is beyond the scope of the current work, we refer the reader to Gray et al. (2020) for a brief discussion on the misspecification of the luminosity function parameters.

¹⁹⁸ The absolute magnitude is related to the intrinsic luminosity of a galaxy by the relation, $M - M^* \equiv -2.5 \log_{10}(L/L^*)$. The parameter M^* of the Schechter function itself depends on H_0 , which we take into account.

Further details and complete derivations for the framework described above are discussed in Gray et al. (2020).

2.3. Posterior Samples Re-weighting

The GW data x_{GW} has undergone parameter estimation, providing a set of posterior samples on source parameters, including the luminosity distance d_L , sky coordinates Ω , and the observed component masses in the detector frame $m_{1,2}^{\text{det}}$. We need the likelihood of the GW data $p(x_{\text{GW}}|H_0)$, which requires removing the priors used for the parameter estimation. In particular, this means that the d_L^2 prior must be removed before the priors on z and H_0 can be applied.

Additionally, a more subtle effect comes into play regarding source- and detector-frame masses. The treatment of GW selection effects requires a marginalization over the source-frame mass distribution, while the data x_{GW} contains information about the detector-frame masses. In order to be self-consistent, the analysis must be performed using the same prior assumptions on both the individual event data and the normalizing $p(D_{\text{GW}}|H_0)$ term. This requires removing the detector-frame mass prior and re-weighting the posterior samples with the source-frame mass prior.

The source-frame mass distribution is $p(m_1, m_2 | \mu)$, where μ denotes the hyper-parameters describing the astrophysical model (concrete details of the assumed model are discussed later in Section 4). To re-weight the likelihood we use the measured detector-frame masses and luminosity distances to compute the corresponding source-frame masses as a function of H_0 ,

$$m_{1,2} = \frac{m_{1,2}^{\text{det}}}{1 + z(d_L, H_0)}. \quad (13)$$

We marginalize out the source-frame mass dependence using the prior $p(m_1, m_2 | \mu)$. The GW likelihood is a function of d_L and Ω as before, but now is also a function of H_0 . This effect will be most pronounced for high distance (redshift) events, where the conversion between detector-frame and source-frame masses is most noticeable. Additionally, posterior samples from events with particularly high or low detector-frame masses may become inconsistent with the source-frame mass prior for certain values of H_0 , leading to additional constraining power (see Section 5.2 for details).

3. Data

3.1. GW Data

The GW searches performed during the first and the second observation runs of the Advanced LIGO and Virgo have led to the identification of 10 BBHs and one BNS merger (Abbott et al. 2019b). The BNS event GW170817, well localized and at a nearby distance of 40_{-10}^{+10} Mpc, helped discover the EM transient from the merger and was subsequently associated with host galaxy NGC4993. The BBHs span a large range of distances from 320_{-110}^{+120} to 2840_{-1360}^{+1400} Mpc and are distributed over the sky with 90% credible regions as low as 39 deg^2 to as high as 1666 deg^2 . A summary of the relevant parameters of all the GW detections are given in Table 1.

For the main results presented in Section 4 of this work, we choose the events which meet the selection criterion of network $S/N > 12$ in at least one of the two pipelines for modeled searches, namely, PyCBC and GstLAL. The sensitivity of the

Table 1

Relevant Parameters of the O1 and O2 Detections: Network S/N for the Search Pipeline (PyCBC/GstLAL) in Which the Signal is the Loudest, 90% Sky Localization Region $\Delta\Omega$ (deg²), Luminosity Distance d_L (Mpc, Median with 90% Credible Intervals), and Estimated Redshift z_{event} (median with a 90% Range Assuming Planck 2015 Cosmology) from Abbott et al. (2019b)

Event	S/N	$\Delta\Omega/\text{deg}^2$	d_L/Mpc	z_{event}	V/Mpc^3	Galaxy Catalog	Number of Galaxies	m_{th}	$p(G z_{\text{event}}, D_{\text{GW}})$
GW150914	24.4	182	440^{+150}_{-170}	$0.09^{+0.03}_{-0.03}$	3.5×10^6	GLADE	3910	17.92	0.42
GW151012	10.0	1523	1080^{+550}_{-490}	$0.21^{+0.09}_{-0.09}$	5.8×10^8	GLADE	78195	17.97	0.01
GW151226	13.1	1033	450^{+180}_{-190}	$0.09^{+0.04}_{-0.04}$	2.4×10^7	GLADE	27677	17.93	0.41
GW170104	13.0	921	990^{+440}_{-430}	$0.20^{+0.08}_{-0.08}$	2.4×10^8	GLADE	42221	17.76	0.01
GW170608	15.4	392	320^{+120}_{-110}	$0.07^{+0.02}_{-0.02}$	3.4×10^6	GLADE	6267	17.84	0.60
GW170729	10.8	1041	2840^{+1400}_{-1360}	$0.49^{+0.19}_{-0.21}$	8.7×10^9	GLADE	77727	17.82	< 0.01
GW170809	12.4	308	1030^{+320}_{-390}	$0.20^{+0.05}_{-0.07}$	9.1×10^7	GLADE	18749	17.62	< 0.01
GW170814	16.3	87	600^{+150}_{-220}	$0.12^{+0.03}_{-0.04}$	4.0×10^6	DES-Y1	31554	23.84	> 0.99
GW170817	33.0	16	40^{+7}_{-15}	$0.01^{+0.00}_{-0.00}$	227
GW170818	11.3	39	1060^{+420}_{-380}	$0.21^{+0.07}_{-0.07}$	1.5×10^7	GLADE	1059	17.51	< 0.01
GW170823	11.5	1666	1940^{+970}_{-900}	$0.35^{+0.15}_{-0.15}$	3.5×10^9	GLADE	117680	17.98	< 0.01

Note. In the remaining columns we report the corresponding 90% 3D localization comoving volumes, the number of galaxies within each volume for public catalogs which we find to be the most complete, and the apparent magnitude threshold, m_{th} , of the galaxy catalog associated with the corresponding sky region (as described in Section 3.3). The final column gives the probability that the host galaxy is inside the galaxy catalog for each event, $p(G|z_{\text{event}}, D_{\text{GW}})$, also evaluated at the median redshift for each event.

results to this choice is explored in Section 5 by reducing the network S/N threshold to 11. In each case, this S/N threshold is also used in the treatment of GW selection effects as described in Equation (3) above. In practice a detection is claimed not solely on the basis of the S/N, but additionally by applying data quality vetoes in order to remove noise transients, and eventually constructing a ranking statistic such as an inverse false alarm rate or a likelihood ratio (Abbott et al. 2019b). A careful treatment should use a threshold on a ranking statistic rather than the S/N as the selection criterion. However a distinction between the two does not cause an appreciable difference if the considered detections are significantly louder than transient noise artifacts (see, e.g., Appendix A.1 of Abbott et al. 2019a). In order to keep the computation of the GW selection effects tractable, one can thus place a more stringent threshold on the S/N and select a subset of loud events from the detected population, which is what we do for our analysis. We note that placing an S/N threshold lower than or close to that set by the detection pipelines would again be problematic without modifications to the current method of accounting for GW selection effects.

3.2. Galaxy Catalogs

The analysis with BBHs is performed in conjunction with appropriate galaxy catalogs. We use the Galaxy List for the Advanced Detector Era (GLADE) catalog (Dálya et al. 2018) as a default, due to its depth and coverage over an extensive region of the sky (see Section 3.2.1). For GW observations that are particularly well localized, certain galaxy catalogs show a clear improvement in completeness over GLADE within the relevant localization volume of the event. In particular, we use the DES Year 1 (Y1A1 GOLD or simply Y1) catalog (Abbott et al. 2018b; Drlica-Wagner et al. 2018) for the analysis of GW170814 (see Section 3.2.2). GW170818 lies within the footprint of the Sloan Digital Sky Survey (SDSS). While not used in this work, galaxy catalogs based on Data Release 14 (Abolfathi et al. 2018) or Data Release 16 (Ahumada et al. 2020) of the SDSS (including curated versions such as the Gravitational Wave Events in Sloan (GWENS) catalog, M. Rahman et al. 2019, in preparation), could be used to

improve the current analysis for events that fall in the SDSS footprint.

In Table 1 we summarize the galaxy catalogs that we use for our analysis for each of the detections, along with the number of galaxies in the 90% error volume calculated from 3D skymaps constructed from posterior samples associated with the data release of Abbott et al. (2019b),¹⁹⁹ and estimates of the probability that the host galaxy is in the catalog, evaluated at the median redshift for each detection assuming a Planck 2015 cosmology.

In the following, we describe in more detail the galaxy catalogs that we use, quantify the probability that the host galaxy for each event is in the galaxy catalog that is used for its analysis, and discuss the assessment of the completeness over the relevant localization volume for the best localized events. Finally, we quantify the uncertainties associated with the photometric measurement of redshifts in some of these catalogs.

3.2.1. GLADE

We use the GLADE version 2.4 galaxy catalog (Dálya et al. 2018),²⁰⁰ to construct the observed redshift distributions for the majority of the detected BBHs. The GLADE catalog has an all sky coverage (Figure 1 of Dálya et al. 2018) since it is constructed from the Gravitational Wave Galaxy Catalogue (GWGC; White et al. 2011), 2MASS Photometric Redshift (2MPZ; Bilicki et al. 2014), Two Micron All Sky Survey (2MASS) Extended Source Catalog (Skrutskie et al. 2006), HyperLEDA (Makarov et al. 2014), and SDSS-DR12Q (Pâris et al. 2017) catalogs. The GLADE catalog is complete (in B -band luminosity) out to 37 Mpc and has an estimated completeness of 50% out to 91 Mpc (Figure 2 of Dálya et al. 2018). At low redshifts ($\lesssim 0.05$), we expect to be dominated by the peculiar-velocity field. GLADE reports peculiar-velocity-corrected redshifts following the reconstruction of Carrick et al. (2015). GLADE provides apparent magnitudes in the B -band,

¹⁹⁹ Available at: <https://www.gw-openscience.org/GWTC-1>.

²⁰⁰ GLADE is publicly available at: <http://glade.elte.hu>.

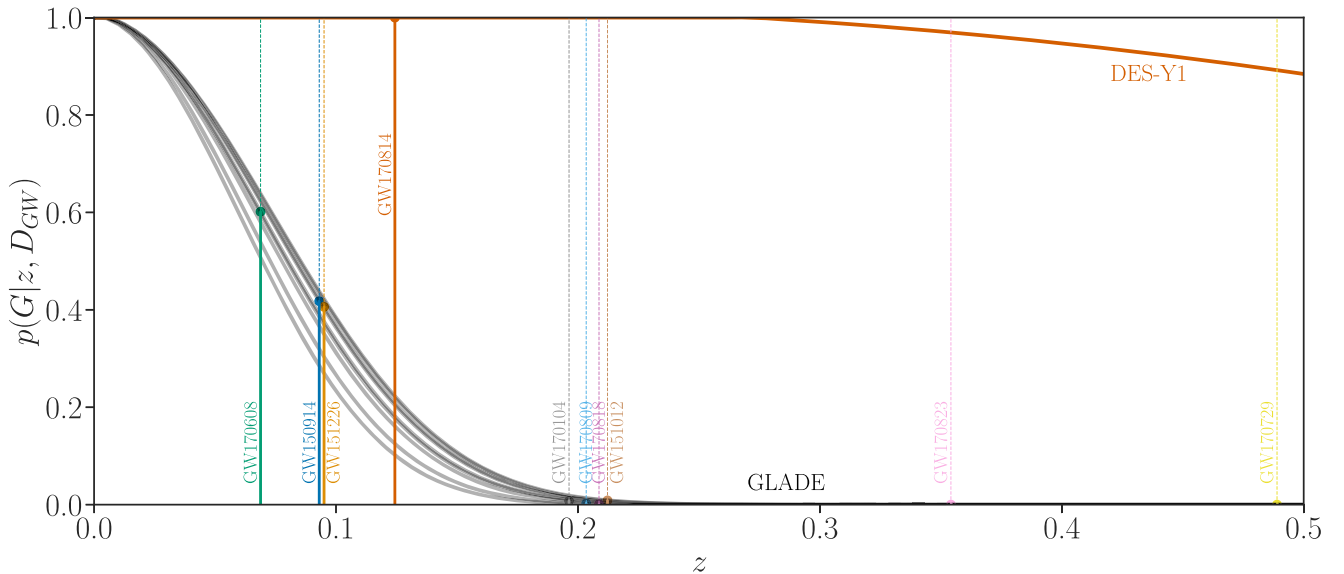


Figure 1. The probability that the host galaxy is inside the galaxy catalog, shown for GLADE (gray curves) and DES-Y1 (orange curve), as a function of redshift. For GLADE, this quantity is calculated for each individual event, using the completeness estimated within each event’s sky localization. For DES-Y1, the curve is only valid in the patch of sky covering GW170814. Each curve is independent of the value of H_0 . The vertical lines show the median redshift (assuming a Planck 2015 cosmology) for each event as in Table 1. These lines are thick and solid up to the intercept with the galaxy catalog they are used with, and thin and dashed above.

which we can use directly (i.e., without any photometric transformations) for luminosity weighting of the galaxies.

3.2.2. DES Year 1

The DES is a 5 yr survey mapping ≈ 300 million galaxies in five filters (*grizY*) over 5000 deg^2 . It is worth noting that the GW170814 sky localization is fully enclosed within the footprint of the SDSS (Drlica-Wagner et al. 2018; Abbott et al. 2018b) Year 3 (Y3) GOLD catalog. An estimate of H_0 from the GW170814 distance and the Y3 catalog of the DES has been carried out (Soares-Santos et al. 2019). In this work, we use the publicly available DES-Y1 catalog (Abbott et al. 2018b)²⁰¹ to compute the H_0 posterior for GW170814. Approximately 87% of the probability region for the GW170814 sky localization is enclosed within the DES-Y1 catalog. Analysis with a different catalog provides a parallel measurement of H_0 with GW170814, and (given the catalog differences) can potentially be indicative of systematic effects in the catalogs, such as the treatment of redshift uncertainties (provided that a similar set of galaxies are present in both catalogs).

We select the objects in the DES-Y1 catalog that are classified as high-confidence galaxies using the default classification scheme, “MODEST_CLASS” (Drlica-Wagner et al. 2018; Sevilla-Noarbe et al. 2018). We use the photometric redshifts that are derived using the Bayesian photometric redshift (BPZ) template fitting method (Hoyle et al. 2018). We use the median redshifts provided in the catalog and discard (around 5%) galaxies with redshift errors larger than twice their corresponding quoted median redshift value. Such a choice is not expected to bias our result since the discarded galaxies are highly uninformative.

We convert from the DES *grizY* magnitudes to the SDSS *ugriz* system using the photometric transformations provided in the DES-Y1 paper (Drlica-Wagner et al. 2018), which requires discarding a further $\sim 5\%$ of galaxies with inadequate color information. This transformation enables us to apply K corrections

to obtain source-frame luminosities (see Section 3.4.2 for details). We use the SDSS *g*-band magnitudes, as these are closest to *B*-band, and update the Schechter parameters of our analysis to have $\alpha = -0.89$ and $M^*(H_0) = -19.39 + 5 \log_{10} h$ based on Blanton et al. (2003).

3.3. Probability That the Host Galaxy is in the Catalog

In this work, we assume that we can characterize the completeness of a galaxy catalog using an apparent magnitude threshold (limiting magnitude) m_{th} . We estimate m_{th} by calculating the median value from the apparent magnitude distribution of all the galaxies within the sky localization of each event. For GLADE, this choice allows us to account for some of the larger changes in completeness across the sky, which come from it being a composite catalog, comprised of many surveys of differing depths. Galaxy catalogs are directional, and a more sophisticated analysis would involve calculating the limiting magnitude for a given line of sight. Obtaining the H_0 posterior distribution would thus require a joint estimate of m_{th} along the lines of sights within an event’s sky localization. We leave this for future work. That the completeness of a galaxy catalog is modeled by a set of limiting magnitude thresholds, can by itself be a nontrivial assumption, especially for photometric catalogs, since galaxies may be missing for various reasons other than them being too faint. This will also need to be revisited in the future in a catalog-specific manner.

For now, we use the m_{th} estimated as described above, and show in Figure 1 the probability of a host galaxy being inside the catalog $p(G|z, D_{\text{GW}})$ as a function of redshift z , for each of the galaxy catalogs under consideration. For GLADE this quantity is calculated for each event using the m_{th} calculated for each event’s sky localization. For DES-Y1, the curve is for the patch of sky covering GW170814. These probabilities are calculated using the expressions in Equation (10), but as a function of z , and are therefore independent of the choice of H_0 . We additionally show as the vertical lines in Figure 1 the median redshift for each event z_{event} (calculated assuming a

²⁰¹ DES-Y1 is available at: <https://des.ncsa.illinois.edu/releases/y1a1>.

Planck 2015 cosmology). In the final two columns of Table 1, we report the m_{th} of the relevant catalog within the sky localization of each event, and the probability of the host galaxy being in the catalog at the median redshift of each event.

3.4. Detailed Analysis of DES-Y1

The high completeness fraction of DES-Y1 within the GW170814 sky localization is apparent from Figure 1. The catalog is expected to be more complete than GLADE since it has a limiting magnitude of approximately 23.8 for DES-Y1. We analyze the EM information coming from this catalog in greater detail. It is helpful to have an assessment of the contribution from potential host galaxies as a function of redshift for these events. In order to quantify this contribution, we perform a treatment analogous to Fishbach et al. (2019) and compute the ratio $p_{\text{cat}}(z)/p_{\text{vol}}(z)$ between the probability distribution for the redshifts of potential host galaxies $p_{\text{cat}}(z)$ and of a uniform in comoving volume distribution of galaxies $p_{\text{vol}}(z)$. When computing $p_{\text{cat}}(z)$, we include all galaxies brighter than $0.05L_g^*$ within the corresponding event’s 99% sky localization region defined as

$$p_{\text{cat}}(z) \equiv \int p(x_{\text{GW}}|\Omega)p_0(z, \Omega)d\Omega, \quad (14)$$

where $p(x_{\text{GW}}|\Omega)$ is the GW likelihood as a function of the sky position Ω (this effectively weights each galaxy with the 2D skymap probability), and $p_0(z, \Omega)$ represents the galaxy catalog contribution, obtained from the distribution of galaxies in the catalog, marginalized over their redshift uncertainties also obtained from the catalog, and weighted by their probability of hosting a GW source (assuming a Planck 2015 cosmology for the required magnitude conversion). We consider weights for each galaxy proportional to their g -band luminosity as well as uniform weights to explore the effects due to this choice.

In Figure 2, we show the distributions $p_{\text{cat}}(z)/p_{\text{vol}}(z)$ for the DES-Y1 galaxies within the GW170814 sky localization region, for the redshift range $0 < z < 0.5$. The unweighted curve traces the over/under-density of galaxies, and then falls off at larger redshift due to incompleteness in the catalog. The luminosity-weighted redshift distribution is driven partially by the overdensity of galaxies at $z \approx 0.4$, and partially by bright high-redshift galaxies. The host galaxies for GW170814 are more likely to be located near the higher galaxy density regions in the DES-Y1 catalog—these features in the redshift prior are expected to drive the inferred H_0 posteriors for the corresponding events. Features we see in the DES-Y1 catalog are not as pronounced as the overdensity in the DES-Y3 data seen in Soares-Santos et al. (2019). While the DES-Y3 survey is deeper, and may reveal finer features, a part of the above difference is likely also driven by the difference in the photometric redshift estimation algorithms, namely, template fitting methods such as BPZ (Hoyle et al. 2018) and machine-learning-based methods such as the ANNz2 algorithm (Sadeh et al. 2016), with the latter used for GW170814 in (Soares-Santos et al. 2019). Only the former of the two has been used for the DES-Y1 catalog and a combination of both for the DES-Y3 catalog. The different selection criteria for choosing galaxies from the two catalogs, such as the stringent redshift cut placed in Soares-Santos et al. (2019) versus a more relaxed redshift prior used in this work, is another potential source of difference between the corresponding redshift distributions.

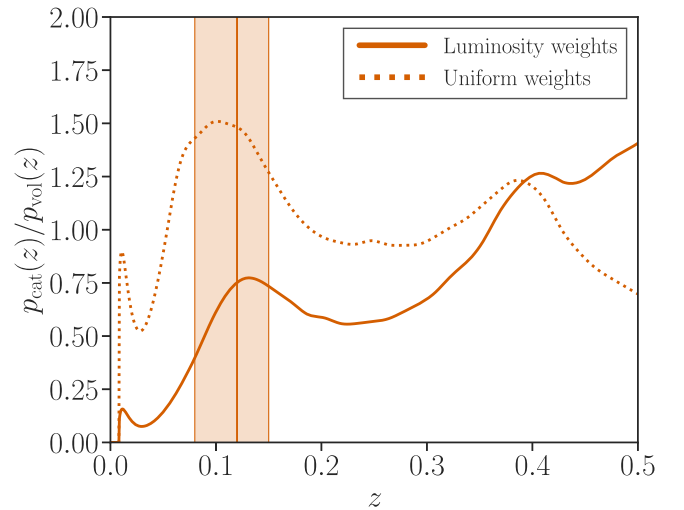


Figure 2. Probability distribution for the redshifts of potential host galaxies $p_{\text{cat}}(z)$, with redshift uncertainties taken into account, divided out by a uniform in comoving volume distribution $p_{\text{vol}}(z)$ of galaxies. When computing $p_{\text{cat}}(z)$ we include all galaxies brighter than $0.05L_g^*$ within the corresponding event’s 99% sky localization region and weight each galaxy by weights proportional to their g -band luminosity (solid lines) as well as with uniform weights (dotted lines). We show these distributions for the DES-Y1 galaxies within the GW170814 sky localization region. We also show the 90% median estimated redshift range for GW170814 (calculated assuming a Planck 2015 cosmology) for reference.

3.4.1. Redshift Uncertainties

An important source of measurement uncertainty with galaxy catalogs is in the galaxy redshifts, which are often photometric estimates due to lack of spectroscopic measurements out to large redshifts. In our formalism, the uncertainty in redshift is reflected in the term $p(z_j)$ in Equation (7). We model the individual galaxy redshift probability distributions, $p(z_j)$, as a Gaussian distribution with the mean set to the quoted median photometric redshift z_{photo} and with a standard deviation of $\sigma_{z_{\text{photo}}}$ (both obtained from the galaxy catalog data). Photometric redshift estimates are often not approximated by Gaussian distributions, and we make this assumption only due to limited information present in some of the public galaxy catalogs that we use. A rigorous quantification of the effect of this assumption is beyond the scope of this work. In practice, we implement the redshift uncertainty by the process of a Monte Carlo integration: the integral over z_j in Equation (7) becomes an additional sum over N_{photo} random samples. This number varies between the different galaxies and is always high enough to ensure that the final event likelihood is independent of the set of random draws from each galaxy.

3.4.2. Source-frame Luminosities

For galaxy catalogs that are complete to high redshifts, it is important to note that the observed apparent magnitudes are redshifted from their source frame. Galaxies do not emit uniformly in all wavelengths, and galaxy surveys are only sensitive in certain bands. In order to compare the properties of galaxies at different redshifts, e.g., to apply luminosity weighting, or to apply a luminosity cut to the galaxy sample, the K correction, described in Oke & Sandage (1968) and Hogg et al. (2002), needs to be applied. In particular, the K correction term is redshift dependent and so neglecting it could lead to systematic bias in the estimation of H_0 .

For DES, we compute the K corrections using the calculator described in Chilingarian et al. (2010) and Chilingarian & Zolotukhin (2012). These K corrections are valid out to redshifts

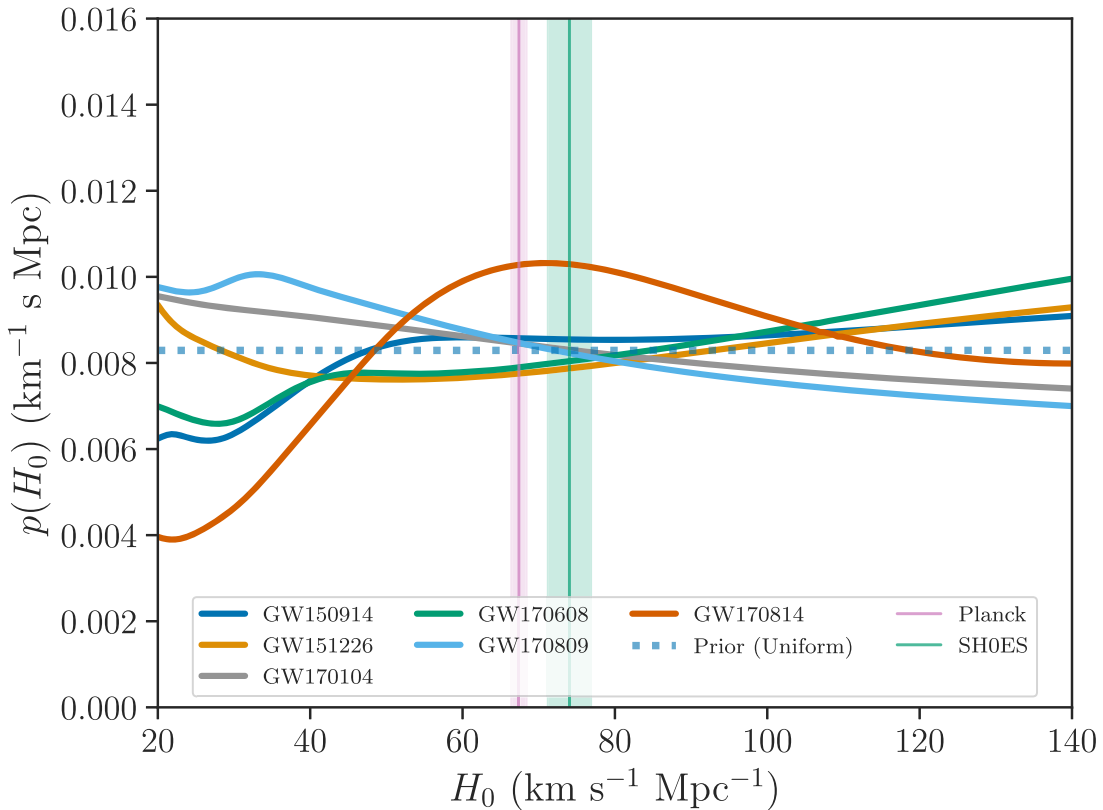


Figure 3. Individual estimates of H_0 from the six BBH detections that satisfy the selection criterion of a network $S/N > 12$ in at least one search pipeline. These results assume a $m^{-1.6}$ power-law distribution on masses and a non-evolving rate model. All results assume a prior on H_0 uniform in the interval $[20, 140]$ $\text{km s}^{-1} \text{Mpc}^{-1}$ (dotted blue). We also show the estimates of H_0 from the cosmic microwave background (CMB; Planck Collaboration et al. 2020) and supernova observations (SH0ES; Riess et al. 2019).

of 0.5 and so we apply a hard redshift cut. In order to remain self-consistent, the method is adjusted to include this redshift cut, such that the probability of the host galaxy being in the catalog above $z = 0.5$ is zero, and below the cut it is determined according to the apparent magnitude threshold, as before.

In the case where galaxies have high redshifts and large redshift uncertainties, this uncertainty must be accounted for in the calculation of the K corrections. Using only the mean redshift to calculate the K correction would lead to unrealistically bright or faint luminosities at the tail ends of the redshift distribution. In our implementation, the K corrections are calculated in situ for each redshift Monte Carlo random draw described in Section 3.4.1, automatically taking the galaxy redshift uncertainties into account.

4. Results

We apply the method described above to obtain a measurement of H_0 using GW standard sirens only. We carry out our analysis with a prior on H_0 uniform in the interval of $[20, 140]$ $\text{km s}^{-1} \text{Mpc}^{-1}$; we report our final results also using a flat-in-log prior $p(H_0) \propto H_0^{-1}$ in the same interval for ease of comparison with previous studies. We use the marginalized distance likelihood and skymaps constructed from the posterior samples of Abbott et al. (2019b).²⁰² For the BBHs, we choose all galaxies in the 99.9% sky region of the corresponding catalog and we further weight the galaxies in proportion to their

$B(g)$ -band luminosities. In order to calculate the term $p(D_{\text{GW}}|H_0)$ in the denominator, we use a Monte Carlo integration, sampling parameters that affect an event’s detectability (masses, sky location, inclination angle, and polarization) from chosen priors. We choose a power-law mass distribution for BBHs with $p(m_1) \propto m_1^{-\alpha}$ and m_2 uniform in its range with $5M_\odot < m_2 < m_1 < 100M_\odot$ in the source frame, and a distribution of merger rates that does not evolve with redshift; for the power-law index α , we choose $\alpha = 1.6$ (which is supported by Model B of Abbott et al. 2019a). For BNSs, we use a Gaussian mass distribution with a mean of $1.35M_\odot$ and a standard deviation of $0.15M_\odot$ (Kiziltan et al. 2013).²⁰³ The remaining GW parameters are marginalized over their natural distributions: uniform in the sky, uniform on the sphere for orientation, uniform in polarization. We use the time-averaged power-spectral-density of detector noise for the corresponding observation run from Abbott et al. (2018a), and for the selection criterion, we use a network S/N threshold of 12 in at least one search pipeline. The O1 and O2 BBHs that pass this criterion are GW150914, GW151226, GW170104, GW170608, GW170809, and GW170814 (see Table 1).

Our result for these O1 and O2 BBHs is shown in Figure 3. The detections for which there is considerable support from the galaxies present in the catalog show features of the galaxy catalog in their H_0 posterior distribution. The GW170814 estimate is qualitatively similar to the result in Soares-Santos

²⁰² For computational convenience, we separately construct a marginalized distance likelihood and a two-dimensional skymap; this approximation will be revisited in the future.

²⁰³ While this does not significantly affect our current results, we will need to revisit the BNS mass distribution in light of GW190425 (Abbott et al. 2020), which is potentially a BNS merger with heavier components.

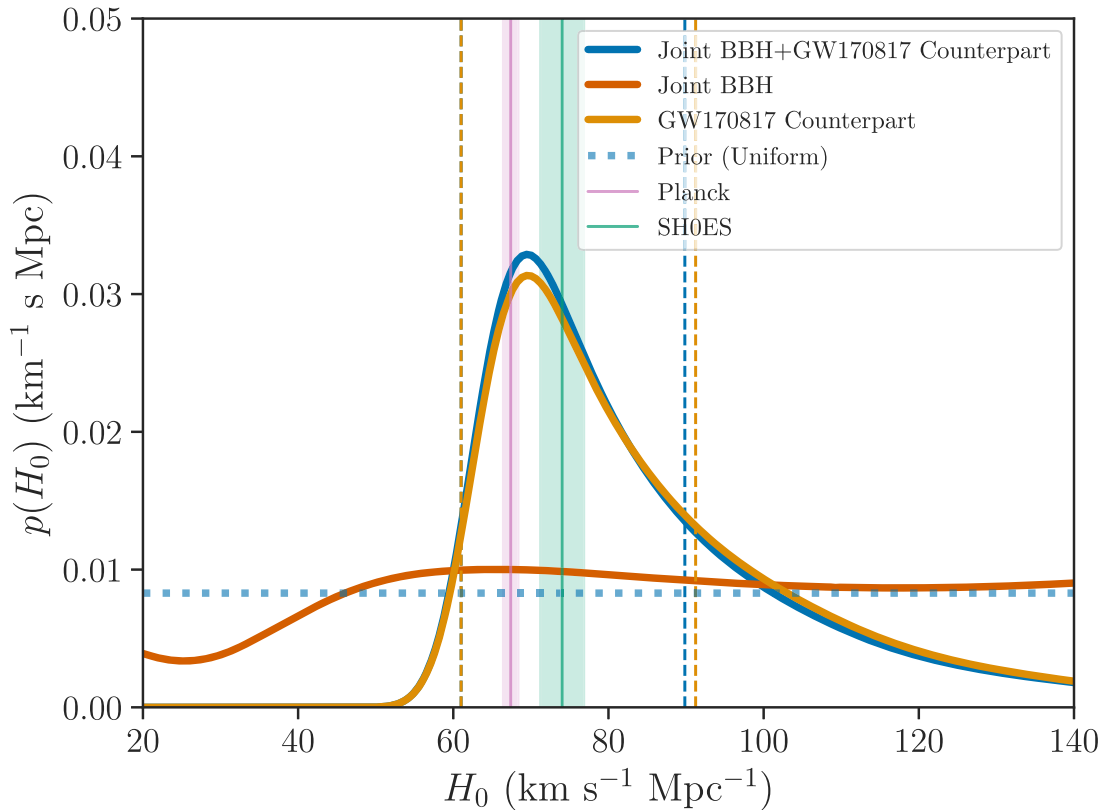


Figure 4. The GW measurement of H_0 (dark blue) from the detections in the first two observing runs of the Advanced LIGO and Virgo. The GW170817 estimate (orange) comes from the identification of its host galaxy NGC4993 (Abbott et al. 2017a). The additional contribution comes from BBHs in association with appropriate galaxy catalogs; for GW170814, we use the DES-Y1 galaxy catalog, while for the remaining five BBHs, GW150914, GW151226, GW170104, GW170608, and GW170809, we use the GLADE catalog. The 68% maximum a posteriori intervals are indicated with the vertical dashed lines. All results assume a prior on H_0 uniform in the interval $[20, 140] \text{ km s}^{-1} \text{ Mpc}^{-1}$ (dotted blue). We also show the estimates of H_0 from the CMB (Planck Collaboration et al. 2020) and supernova observations (SH0ES: Riess et al. 2019).

et al. (2019) with analogous peaks in the posterior distribution. The differences in peak locations can be attributed to a difference in the redshift distribution for the DES-Y3 catalog used in Soares-Santos et al. (2019) versus that for the public DES-Y1 catalog used in this work. For the detections for which the galaxy catalogs are relatively empty, we see the features of the assumptions on mass distribution and redshift evolution of binary merger rate that have entered our analysis. The more distant events, such as GW170809, lead to H_0 estimates pushed to the lower end of the prior. This is due to the following reason. In a universe where host galaxies are distributed uniformly in comoving volume, for lower values of H_0 , the expected distribution of detected GW events favors relatively higher luminosity distances. Thus, events at high luminosity distances have more support for smaller values of H_0 , while relatively nearby events, namely, GW150914, GW151226, GW170608, and GW170814, correspondingly, have lower support at smaller values of H_0 . The information present in the observed luminosity distance distribution would thereby potentially contribute to the H_0 measurement, independent of, or even in absence of information in galaxy catalogs, if the underlying distributions of source parameters were known.

In the absence of knowledge of the astrophysical distribution of BBH source parameters, a thorough treatment would involve a marginalization over all possible mass distributions and rate models. The following section discusses the systematic differences that the assumptions on the assumed population model could lead to.

For our final result we combine the contribution of the BBHs with the result from GW170817 obtained using the low spin prior samples from Abbott et al. (2019b) and an estimated Hubble velocity of $v_H \equiv cz = 3017 \pm 166 \text{ km s}^{-1}$ (where c is the speed of light) for NGC4993 from Abbott et al. (2017a). Our final combined result is shown in Figure 4, with the posterior distribution plotted assuming a uniform H_0 prior: we obtain $H_0 = 70_{-9}^{+20} \text{ km s}^{-1} \text{ Mpc}^{-1}$ (68.3% highest density posterior interval). To compare with values in the literature, we also use a flat-in-log prior, $p(H_0) \propto H_0^{-1}$, and calculate $H_0 = 69_{-8}^{+16} \text{ km s}^{-1} \text{ Mpc}^{-1}$, which corresponds to an improvement by a factor of 1.04 (about 4%) over the GW170817-only value of $69_{-8}^{+17} \text{ km s}^{-1} \text{ Mpc}^{-1}$. We also quote the median and symmetric 90% credible interval for this measurement, which is $75_{-14}^{+39} \text{ km s}^{-1} \text{ Mpc}^{-1}$.

5. Systematic Effects

In this section, we repeat the previous analysis with a few alternative assumptions for the GW selection criterion, the GW population model, and source host properties. Subsequently, we discuss other sources of systematic effects, a detailed study of which is beyond the scope of this work.

5.1. Selection Criterion

We first look into the sensitivity of our results to the GW selection criterion. We reduce the threshold on the network S/N from 12 chosen in the previous section to 11 in at least one search

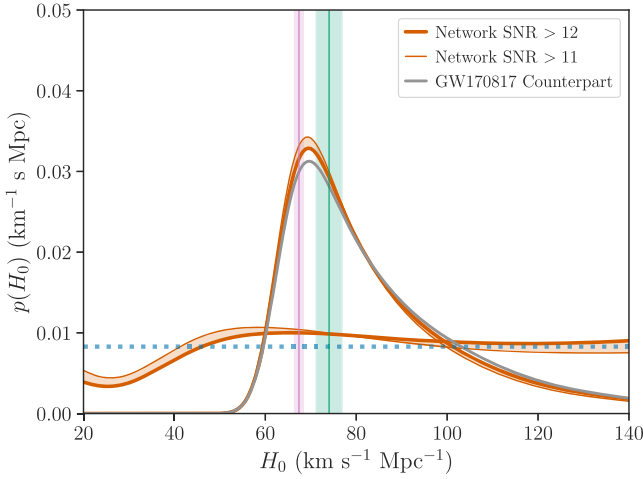


Figure 5. Sensitivity of the results to the selection criterion on the S/N. The final joint result as well as the contribution from all the BBHs that satisfy the selection criterion are shown for a threshold network S/N of 12 (thick orange) and 11 (thin orange); the variation is shown as a shaded band. The GW170817 counterpart result (gray) is added to guide the eye. Six BBHs (GW150914, GW151226, GW170104, GW170608, GW170809, and GW170814) pass the selection criterion with an S/N > 12. Two additional BBHs (GW170818 and GW170823) are included with an S/N > 11. These results assume the default $m^{-1.6}$ power-law distribution on masses and a non-evolving rate model.

pipeline. The computation of the GW selection effects is adjusted accordingly. Figure 5 shows the results with the two sets of assumptions. Reducing the S/N threshold to 11 introduces two additional events in our analysis, namely, GW170818 and GW170823, neither of which have a significant in-catalog contribution. Differences are expected due to the fact that additional low-S/N events are introduced, and also because the individual likelihoods change slightly with a different S/N threshold used in the GW selection term. In the regime of a large number of events, these two effects are expected to cancel, provided that the additional low-S/N events do not have significant in-catalog support. For our result, this difference is not significant; however, the small variation is a reminder that we are still in the regime of a low number of events.

5.2. Population Model

Going back to our default assumption of a network S/N threshold of 12, we test the sensitivity to our assumptions regarding the population model, i.e., the mass distribution and the distribution of binary merger rate with redshift. In addition to the power-law mass distribution with $\alpha = 1.6$ (median inferred value using Model B of Abbott et al. 2019a), we choose a shallower flat-in-log mass distribution with $\alpha = 1$, and a steeper distribution with $\alpha = 2.3$ (both within the support of the inferred range in Abbott et al. 2019a). Our results are shown in the left panel of Figure 6, and they demonstrate that the systematic differences due to the choice of power-law slope α are insignificant.

As a test case, we vary the upper cutoff for the mass distribution, M_{\max} . For our default analysis, M_{\max} was chosen to be $100 M_{\odot}$, consistent with all the considered BBHs for all values of H_0 within the prior range. Reducing this cutoff to a slightly restrictive $M_{\max} = 50 M_{\odot}$ (e.g., motivated by the pair instability supernova process, Fowler & Hoyle 1964), we see a significant difference (right panel of Figure 6). Lowering M_{\max} corresponds to a closer GW detection horizon. This

systematically leads each event to prefer slightly lower values of H_0 than in the main result, for the reasons outlined in Section 4, namely, the relationship between the predicted event distribution (from our GW selection effects) and the real detected event distribution.

Next, we relax our assumption on the evolution of rate of binary mergers with redshift. A constant merger rate density, $R(z) = \text{constant}$, implicit in the previous treatment, assumed that the merger rate traces the comoving volume. In addition, we repeat our analysis using a merger rate $R(z) \propto (1+z)^3$ that traces the star formation rate at low redshifts ($z < 2.5$) (Saunders et al. 1990), as well as a merger rate $R(z) \propto (1+z)^{-3}$ that could arise if typical delay times are very long, as may be expected from the chemically homogeneous evolution formation channel (Mandel & de Mink 2016). These relaxed assumptions thus cover a large fraction of physically viable and inferred population models (Abbott et al. 2019a). We show our results for the different assumed redshift evolution models in Figure 7. The model in which the merger rate traces star formation shows a significant difference, with a tendency to prefer lower values of H_0 , compared to the other two models which are quite similar. This is the only systematic effect that leads to a significant difference in the results at this time.

5.3. Luminosity Weighting

The results in the previous section assumed a weighting of galaxies by their luminosities in the *B*-band, which are indicative of galaxies' star formation rates. Luminosities in the infrared (such as the *K*-band) are more indicative of the total masses of galaxies; however, infrared luminosities are not present in catalogs like DES-Y1. In order to quantify the difference likely to be caused by alternate ways of weighting the galaxies, we repeat our analysis with no luminosity weighting. These results are shown in Figure 8.

With uniform luminosity weights, we obtain a result on a joint BBH estimate that is close to flat (thin orange line in Figure 8). This can be understood as follows: (1) The out-of-catalog terms in Equation (6) take into account the lack of galaxies beyond the apparent magnitude threshold m_{th} of the catalog in a uniform way. When galaxies are unweighted, the probability of the host galaxy being inside the catalog is reduced compared to the luminosity-weighted case. More weight is given to the uniform out-of-catalog contribution, and the events become less informative. (2) The catalogs used in this analysis contain high numbers of low-luminosity galaxies. The contribution from these more evenly distributed dim galaxies, in the unweighted case, again reduces the informativeness of each event and flattens the final result. This is also in agreement with our expectations from Fishbach et al. (2019) and Gray et al. (2020), where weighting by luminosities enhance the features in the posterior distribution coming from the galaxy catalog.

5.4. Waveform Models

The posterior samples of Abbott et al. (2019b) used for the results in this paper have been obtained combining the results of gravitational waveform models that incorporate spin and precession effects to different extents (Hannam et al. 2014; Pan et al. 2014; Taracchini et al. 2014; Husa et al. 2016; Khan et al. 2016; Babak et al. 2017). These models are restricted to quasi-circular orbits (i.e., they do not include orbital eccentricity) and

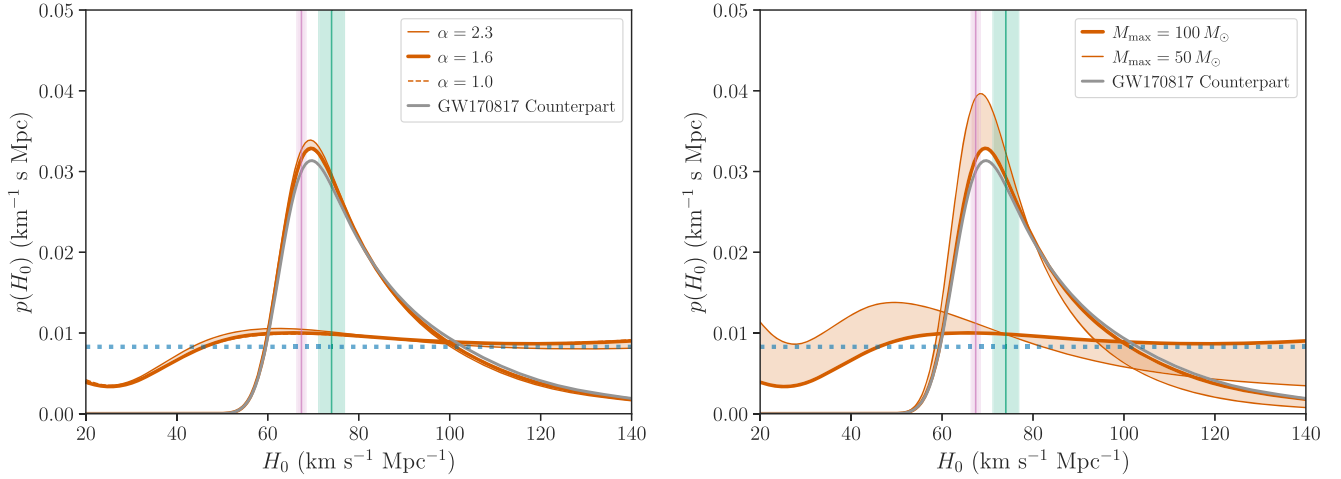


Figure 6. Sensitivity of the results to the assumed mass distribution model. Left panel: variation of the results with three different choices of the power-law index for the mass distribution, $\alpha = 1.6$ (thick solid), $\alpha = 2.3$ (thin solid), and $\alpha = 1$ (thin dashed), assuming a constant intrinsic astrophysical merger rate, $R(z) = \text{constant}$ and $M_{\text{max}} = 100 M_{\odot}$. Right panel: variation of the results with two different choices for the allowed black hole maximum mass, $M_{\text{max}} = 100 M_{\odot}$ (thick solid) and $M_{\text{max}} = 50 M_{\odot}$ (thin solid), both assuming $R(z) = \text{constant}$ and $\alpha = 1.6$.

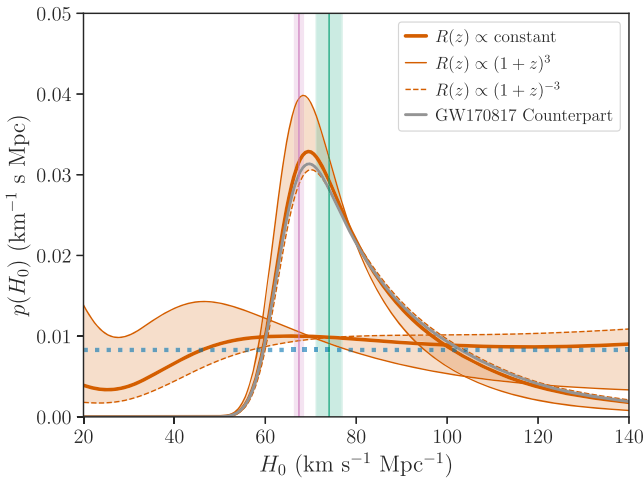


Figure 7. Variation of the results with two different choices for the rate evolution, $R(z) = \text{constant}$ (thick solid), and $R(z) \propto (1+z)^3$ (thin solid) and $R(z) \propto (1+z)^{-3}$ (thin dashed) for $\alpha = 1.6$ and $M_{\text{max}} = 100 M_{\odot}$.

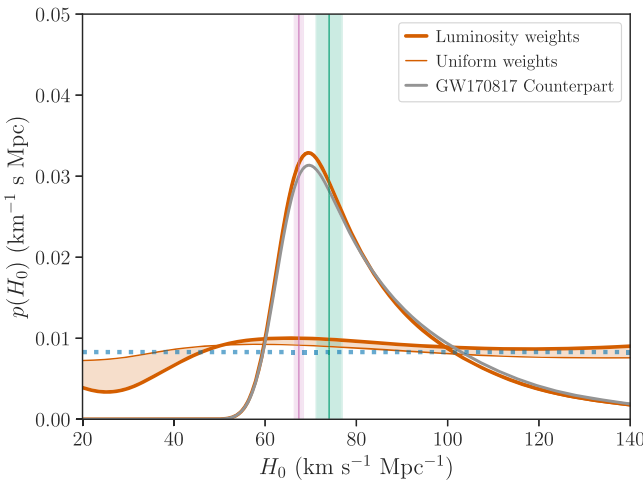


Figure 8. Sensitivity of the results to luminosity weighting. We show how the results vary when we weight the galaxies in the catalog by their $B(g)$ -band luminosity (thick solid) as well as with constant (uniform) weights (thin solid), both assuming a power-law index for the mass distribution, $\alpha = 1.6$, and constant intrinsic astrophysical merger rate, $R(z) = \text{constant}$.

neglect higher-order harmonics. Systematic differences in GW parameter estimation results with the employed waveform models constitute only a small fraction of the total uncertainty budget (see, e.g., Abbott et al. 2016a, 2017b), and given the large statistical uncertainties, the ignored effects in waveform modeling are not expected to cause a difference in the current measurement of H_0 . However cumulative systematic effects arising from limitations of waveform models will become increasingly important as the statistical uncertainties become smaller, and in particular, features that can lead to biases in the GW estimation of distance will need to be incorporated.

5.5. Detector Calibration

An independent effect to be considered is the calibration of the GW detectors. Currently, the GW parameter estimation results are marginalized over the detector calibration uncertainties ($\lesssim 4\%$ in amplitude in O1 and O2), which accounts for both the statistical uncertainty and the systematic error correlated between detections (Abbott et al. 2019b). Both the statistical uncertainty and the systematic error in GW detector calibration are much smaller than the other measurement uncertainties, and thus negligible for H_0 estimates from a handful of detections that we have now or expect in the near future (Cahillane et al. 2017). However, the impact of correlated systematic calibration errors between detections will become relatively more important in the long term, with an increasing number of detections driving down the statistical uncertainties, and an improved understanding of other systematic effects that possibly govern our current uncertainty budget. Further quantitative study of the effect of correlated calibration uncertainties is ongoing.

6. Conclusion and Outlook

In this paper we have presented the first measurement of H_0 using multiple GW observations. Our result reanalyzes and combines the posterior probability distribution obtained from the BNS event GW170817 using the redshift of the host galaxy inferred from the observed EM counterpart (Abbott et al. 2017a), along with constraints using galaxy catalogs for the BBH events observed by the Advanced LIGO and Virgo in

their first and second observing runs. We measure $H_0 = 69^{+16}_{-8}$ km s⁻¹ Mpc⁻¹ (68.3% highest density posterior interval with a flat-in-log prior). This result is mainly dominated by the information from GW170817 with its counterpart, but does show a modest improvement with the inclusion of the BBHs. The BBHs contribute both from associated galaxy catalogs as well as via their observed luminosity distance distribution. Since the latter contribution is sensitive to the assumptions on the mass distribution and rate evolution, a more thorough treatment requires a marginalization over these unknown population parameters.

The contribution from events without counterparts is dominated by GW170814, for which the associated galaxy catalog is highly complete. This highlights the importance of deeper surveys and of dedicated EM follow-up of sky regions following GW triggers for a better H_0 measurement. With numerous anticipated detections in the upcoming observing runs with improved detector sensitivities (Abbott et al. 2016a, 2016b, 2017c, 2018a, 2019a, 2019b), these results pave the way toward an era of precision multimessenger cosmology to be performed with a multitude of sources, including both neutron star and black hole mergers, with or without transient EM counterparts.

Analyses in this paper made use of NUMPY (Harris et al. 2020), SCIPY (Virtanen et al. 2020), ASTROPY (Astropy Collaboration et al. 2013, 2018), GWCOSMO (<https://git.ligo.org/lscsoft/gwcosmo>), and IPYTHON (Perez & Granger 2007); plots were produced with MATPLOTLIB (Hunter 2007), and SEABORN (Waskom et al. 2017). This research made use of the K -corrections calculator service available at <http://kcor.sai.msu.ru/>.

The authors gratefully acknowledge the support of the United States National Science Foundation (NSF) for the construction and operation of the LIGO Laboratory and Advanced LIGO as well as the Science and Technology Facilities Council (STFC) of the United Kingdom, the Max-Planck-Society (MPS), and the State of Niedersachsen/Germany for support of the construction of the Advanced LIGO and construction and operation of the GEO600 detector. Additional support for the Advanced LIGO was provided by the Australian Research Council. The authors gratefully acknowledge the Italian Istituto Nazionale di Fisica Nucleare (INFN), the French Centre National de la Recherche Scientifique (CNRS), and the Foundation for Fundamental Research on Matter supported by the Netherlands Organisation for Scientific Research, for the construction and operation of the Virgo detector and the creation and support of the EGO consortium. The authors also gratefully acknowledge research support from these agencies as well as by the Council of Scientific and Industrial Research of India, the Department of Science and Technology, India, the Science & Engineering Research Board (SERB), India, the Ministry of Human Resource Development, India, the Spanish Agencia Estatal de Investigación, the Vicepresidència i Conselleria d'Innovació Recerca i Turisme and the Conselleria d'Educació i Universitat del Govern de les Illes Balears, the Conselleria d'Educació Investigació Cultura i Esport de la Generalitat Valenciana, the National Science Centre of Poland, the Swiss National Science Foundation (SNSF), the Russian Foundation for Basic Research, the Russian Science Foundation, the European Commission, the European Regional Development Funds (ERDF), the Royal Society, the Scottish Funding Council, the Scottish Universities Physics Alliance, the Hungarian Scientific Research Fund (OTKA), the Lyon Institute

of Origins (LIO), the Paris Île-de-France Region, the National Research, Development and Innovation Office Hungary (NKFIH), the National Research Foundation of Korea, Industry Canada and the Province of Ontario through the Ministry of Economic Development and Innovation, the Natural Science and Engineering Research Council Canada, the Canadian Institute for Advanced Research, the Brazilian Ministry of Science, Technology, Innovations, and Communications, the International Center for Theoretical Physics South American Institute for Fundamental Research (ICTP-SAIFR), the Research Grants Council of Hong Kong, the National Natural Science Foundation of China (NSFC), the Leverhulme Trust, the Research Corporation, the Ministry of Science and Technology (MOST), Taiwan and the Kavli Foundation. The authors gratefully acknowledge the support of the NSF, STFC, INFN, and CNRS for provision of computational resources.

References

- Abbott, B. P., Abbott, R., Abbott, T. D., et al. 2016a, *PhRvX*, **6**, 041015 [Erratum: *Phys.Rev.X* **8**, 039903 (2018)]
- Abbott, B. P., Abbott, R., Abbott, T. D., et al. 2016b, *ApJL*, **833**, L1
- Abbott, B. P., Abbott, R., Abbott, T. D., et al. 2017a, *Natur*, **551**, 85
- Abbott, B. P., Abbott, R., Abbott, T. D., et al. 2017b, *CQGrA*, **34**, 104002
- Abbott, B. P., Abbott, R., Abbott, T. D., et al. 2017c, *PhRvL*, **119**, 161101
- Abbott, B. P., Abbott, R., Abbott, T. D., et al. 2018a, *LRR*, **21**, 3
- Abbott, B. P., Abbott, R., Abbott, T. D., et al. 2019a, *ApJL*, **882**, L24
- Abbott, B. P., Abbott, R., Abbott, T. D., et al. 2019b, *PhRvX*, **9**, 031040
- Abbott, B. P., Abbott, R., Abbott, T. D., et al. 2020, *ApJL*, **892**, L3
- Abbott, T. M. C., Abdalla, F. B., Allam, S., et al. 2018b, *ApJS*, **239**, 18
- Abolfathi, B., Aguado, D. S., Aguilar, G., et al. 2018, *ApJS*, **235**, 42
- Ahumada, R., Prieto, C. A., Almeida, A., et al. 2020, *ApJS*, **249**, 3
- Astropy Collaboration, Price-Whelan, A., Sipőcz, B. M., et al. 2018, *AJ*, **156**, 123
- Astropy Collaboration, Robitaille, T. P., Tollerud, E. J., et al. 2013, *A&A*, **558**, A33
- Babak, S., Taracchini, A., & Buonanno, A. 2017, *PhRvD*, **95**, 024010
- Bilicki, M., Jarrett, T. H., Peacock, J. A., Cluver, M. E., & Steward, L. 2014, *ApJS*, **210**, 9
- Birrer, S., Treu, T., Rusu, C. E., et al. 2019, *MNRAS*, **484**, 4726
- Blanton, M. R., Hogg, D. W., Bahcall, N. A., et al. 2003, *ApJ*, **592**, 819
- Caditz, D., & Petrosian, V. 1989, *ApJL*, **337**, L65
- Cahillane, C., Betziewieser, J., Brown, D. A., et al. 2017, *PhRvD*, **96**, 102001
- Carrick, J., Turnbull, S. J., Lavaux, G., & Hudson, M. J. 2015, *MNRAS*, **450**, 317
- Chen, H.-Y., Fishbach, M., & Holz, D. E. 2018, *Natur*, **562**, 545
- Chen, H.-Y., & Holz, D. E. 2014, arXiv:1409.0522
- Chilingarian, I. V., Melchior, A.-L., & Zolotukhin, I. Y. 2010, *MNRAS*, **405**, 1409
- Chilingarian, I. V., & Zolotukhin, I. Y. 2012, *MNRAS*, **419**, 1727
- Dalal, N., Holz, D. E., Hughes, S. A., & Jain, B. 2006, *PhRvD*, **74**, 063006
- Dálya, G., Galgóczi, G., Dobos, L., et al. 2018, *MNRAS*, **479**, 2374
- Del Pozzo, W. 2012, *PhRvD*, **86**, 043011
- Drlica-Wagner, A., Sevilla-Noarbe, I., Rykoff, E. S., et al. 2018, *ApJS*, **235**, 33
- Farr, W. M., Fishbach, M., Ye, J., & Holz, D. 2019, *ApJL*, **883**, L42
- Feeney, S. M., Peiris, H. V., Williamson, A. R., et al. 2019, *PhRvL*, **122**, 061105
- Finn, L. S. 1994, *PhRvL*, **73**, 1878
- Fishbach, M., Gray, R., Magaña Hernandez, I., Qi, H., & Sur, A. 2019, *ApJL*, **871**, L13
- Fishbach, M., Holz, D. E., & Farr, W. M. 2018, *ApJL*, **863**, L41
- Fowler, W. A., & Hoyle, F. 1964, *ApJS*, **9**, 201
- Gehrels, N., Cannizzo, J. K., Kanner, J., et al. 2016, *ApJ*, **820**, 136
- Gray, R., Hernandez, I. M., Qi, H., et al. 2020, *PhRvD*, **101**, 122001
- Hannam, M., Schmidt, P., Bohé, A., et al. 2014, *PhRvL*, **113**, 151101
- Harris, C. R., Millman, K. J., van der Walt, S. J., et al. 2020, *Natur*, **585**, 357
- Hogg, D. W., Baldray, I. K., Blanton, M. R., & Eisenstein, D. J. 2002, arXiv: astro-ph/0210394
- Holz, D. E., & Hughes, S. A. 2005, *ApJ*, **629**, 15
- Hoyle, B., Gruen, D., Bernstein, G. M., et al. 2018, *MNRAS*, **478**, 592
- Hunter, J. D. 2007, *CSE*, **9**, 90
- Husa, S., Khan, S., Hannam, M., et al. 2016, *PhRvD*, **93**, 044006

- Khan, S., Husa, S., Hannam, M., et al. 2016, [PhRvD](#), **93**, 044007
- Kiziltan, B., Kottas, A., De Yoreo, M., & Thorsett, S. E. 2013, [ApJ](#), **778**, 66
- Macaulay, E., Nichol, R. C., Bacon, D., et al. 2019, [MNRAS](#), **486**, 2184
- MacLeod, C. L., & Hogan, C. J. 2008, [PhRvD](#), **77**, 043512
- Madgwick, D. S., Lahav, O., Baldry, I. K., et al. 2002, [MNRAS](#), **333**, 133
- Makarov, D., Prugniel, P., Terekhova, N., Courtois, H., & Vauglin, I. 2014, [A&A](#), **570**, A13
- Mandel, I., & de Mink, S. E. 2016, [MNRAS](#), **458**, 2634
- Mandel, I., Farr, W. M., & Gair, J. R. 2019, [MNRAS](#), **486**, 1086
- Messenger, C., & Read, J. 2012, [PhRvL](#), **108**, 091101
- Mortlock, D. J., Feeney, S. M., Peiris, H. V., Williamson, A. R., & Nissanke, S. M. 2019, [PhRvD](#), **100**, 103523
- Nair, R., Bose, S., & Saini, T. D. 2018, [PhRvD](#), **98**, 023502
- Nissanke, S., Holz, D. E., Dalal, N., et al. 2013, arXiv:1307.2638
- Nissanke, S., Holz, D. E., Hughes, S. A., Dalal, N., & Sievers, J. L. 2010, [ApJ](#), **725**, 496
- Oke, J. B., & Sandage, A. 1968, [ApJ](#), **154**, 21
- Pan, Y., Buonanno, A., Taracchini, A., et al. 2014, [PhRvD](#), **89**, 084006
- Pâris, I., Petitjean, P., Ross, N. P., et al. 2017, [A&A](#), **597**, A79
- Perez, F., & Granger, B. E. 2007, [CSE](#), **9**, 21
- Planck Collaboration 2016, [A&A](#), **594**, A13
- Planck Collaboration, Aghanim, N., Akrami, Y., et al. 2020, [A&A](#), **641**, A6
- Riess, A. G., Casertano, S., Yuan, W., Macri, L. M., & Scolnic, D. 2019, [ApJ](#), **876**, 85
- Sadeh, I., Abdalla, F. B., & Lahav, O. 2016, [PASP](#), **128**, 104502
- Sathyaprakash, B. S., Schutz, B. F., & Van Den Broeck, C. 2010, [CQGra](#), **27**, 215006
- Saunders, W., Rowan-Robinson, M., Lawrence, A., et al. 1990, [MNRAS](#), **242**, 318
- Schutz, B. F. 1986, [Natur](#), **323**, 310
- Sevilla-Noarbe, I., Hoyle, B., Marchã, M. J., et al. 2018, [MNRAS](#), **481**, 5451
- Skrutskie, M. F., Cutri, R. M., Stiening, R., et al. 2006, [AJ](#), **131**, 1163
- Soares-Santos, M., Palmese, A., et al. 2019, [ApJL](#), **876**, L7
- Taracchini, A., Buonanno, A., Pan, Y., et al. 2014, [PhRvD](#), **89**, 061502
- Taylor, S. R., & Gair, J. R. 2012, [PhRvD](#), **86**, 023502
- Taylor, S. R., Gair, J. R., & Mandel, I. 2012, [PhRvD](#), **85**, 023535
- Virtanen, P., Gommers, R., Oliphant, T. E., et al. 2020, [Nature Methods](#), **17**, 261
- Vitale, S., & Chen, H.-Y. 2018, [PhRvL](#), **121**, 021303
- Vitale, S., Gerosa, D., Farr, W. M., & Taylor, S. R. 2020, arXiv:2007.05579
- Waskom, M., Botvinnik, O., Ostblom, J., et al. 2017, Mwaskom/Seaborn: v0.8.1, Zenodo, doi:10.5281/zenodo.883859
- White, D. J., Daw, E. J., & Dhillon, V. S. 2011, [CQGra](#), **28**, 085016